研究成果の刊行に関する一覧表

雑誌

発表者氏名	論文タイトル名	発表誌名	巻号	ページ	出版年
Ishida K., Kotake Y., Miyara M., Aoki K., Sanoh S., Kanda Y., Ohta S.	Involvement of GluR2 decrease in lead-induced neuronal cell death.	J. Toxicol. Sci.	38	513-521	2013
Yamada S., Kotake Y., Sekino Y., Kanda Y.	AMP-activated protein kinase-mediated glucose transport as a novel target of tributyltin in human embryonic carcinoma cells	Metallomics	5	484-491	2013
関野祐子、佐藤薫、諫田泰成、石田誠一	ヒトiPS分化細胞を利用した医薬品のヒト特異的有害反応評価系の開発・標準化	国立医薬品食品衛生研究所報告	131	25-34	2013
諫田泰成	ヒトiPS細胞から心筋細胞への分化誘導法	日本薬理学雑誌	141	32-36	2013
Yamada S., Kotake Y., Demizu Y., Kurihara M.,Sekino Y., Kanda Y.	Isocitrate dehydrogenase 3 as a novel target of tributyltin in human embryonic carcinoma cells.	Sci. Rep.	4	5952	2014
Nagakubo T., Demizu Y., Kanda Y., Misawa T., Shoda T., Okuhira K., Sekino Y., Naito M., Kurihara M.	Development of cell-penetrating R7 fragment-conjugated helical peptides as inhibitors of estrogen receptor-mediated transcription.	Bioconjugate Chem.	25	1921-1924	2014
Hirata N., Yamada S., Shoda T., Kurihara M., Sekino Y., Kanda Y.	Sphingosine-1-phosphate promotes expansion of cancer stem cells via S1PR3 by a ligand-independent Notch activation	Nature Commun.	5	4806	2014
Hayakawa T., Kunihiro T., Ando T., Kobayashi S., Matsui E., Yada H., Kanda Y., Kurokawa J., Furukawa T.	Image-based evaluation of contraction-relaxation kinetics of human-induced pluripotent stem cell-derived cardiomyocytes: correlation and complementarity with extracellular electrophysiology.	J. Mol. Cell. Cardiol.	77	178-191	2014
Hiyoshi H., Goto N., Tsuchiya M., Iida K., Nakajima Y., Hirata N., Kanda Y., Nagasawa K., Yanagisawa J.	YL-109 is a novel antitumor agent suppressing triple-negative breast cancer progression by inducing ubiquitin ligase CHIP.	Sci. Rep.	4	7095	2014
Tsuchiya M, Nakajima Y, Hirata N, Morishita T, Kishimoto H, Kanda Y, Kimura K.	Ubiquitin ligase CHIP suppresses cancer stem cell properties in a population of breast cancer cells.	Biochem Biophys Res Commun.	452	928-932	2014
Nakamura Y., Matsuo J., Miyamoto N., Ojima A., Ando K., Kanda Y., Sawada K., Sugiyama A., Sekino Y.	Assessment of testing methods for drug-induced repolarization delay and arrhythmias in an iPS cell-derived cardiomyocyte sheet: multi-site validation study.	J Pharmacol Sci.	124	494-501	2014
諫田泰成	ヒトiPS細胞を用いた成熟心筋細胞の開発	心電図	34	306-309	2014

澤田光平、松尾純子、長田智治、吉田善紀、白尾智明、佐藤薫、諫田泰成、関野祐子	霧島会議Stem Cell Safety Pharmacology Working Groupまとめ－ヒトES/iPS細胞由来心筋細胞を用いた催不整脈作用検出とその課題－	心電図	34	302-305	2014
諫田泰成	癌幹細胞の受容体を標的とした創薬の可能性	日本薬理学雑誌	144	17-21	2014
Yosuke D, Takashi Mi, Takaya N, Yasunari K, Keiichiro O, Yuko S, Mikihiko N, Masaaki K.	Structural development of stabilized helical peptides as inhibitors of estrogen receptor (ER)-mediated transcription.	Bioorg.Med.Chem.	23	4132-8	2015
Asakura K, Hayashi S, Ojima A, Taniguchi T, Miyamoto N, Nakamori C, Nagasawa C, Kitamura T, Osada T, Honnda Y, Kasai C, Ando H, Kanda Y, Sekino Y, Sawada K.	Improvement of acquisition and analysis methods in multi-electrode array experiments with iPS cell-derived cardiomyocyte.	Journal of Pharmacological and Toxicological Methods			2015
Yamada S., Kotake Y., Nakano M., Sekino Y. Kanda Y.	Tributyltin induces mitochondrial fission through NAD-IDH dependent mitofusin degradation in human embryonic carcinoma cells.	Metallomics	7	1240-6	2015
Asanagi M., Yamada S., Hirata N, Itagaki H., Kotake Y., Sekino Y. Kanda Y.	Tributyltin induces G2/M cell cycle arrest via NAD+-dependent isocitrate dehydrogenase in human embryonic carcinoma cells.	JTS	41	207-215	2016
Hirata N., Yamada S., Asanagi M., Sekino Y., Kanda Y.	Nicotine induces mitochondrial fission through mitofusin degradation in human multipotent embryonic carcinoma cells.	BBRC	470	300-5	2016
Kim S.-R., Kubo T., Kuroda Y., Hojyo M., Matsuo T., Miyajima A., Usami M., Sekino Y., Matsushita T., Ishida S.	Comparative metabolome analysis of cultured fetal and adult hepatocytes in humans.	J Toxicol Sci.	39	717-723	2014
Usami M., Mitsunaga K., Irie T., Miyajima A., Doi O.	Simple in vitro migration assay for neural crest cells and the opposite effects of all-trans-retinoic acid on cephalic- and trunk-derived cells.	Congenit Anom	54	184-188	2014
Usami M., Mitsunaga K., Irie T. Nakajima M.	Various definitions of reproductive indices: a proposal for combined use of brief definitions.	Congenital Anomalies	54	67-68	2014

Usami M., Mitsunaga K., Irie T., Miyajima A. Doi O.	Proteomic analysis of ethanol-induced embryotoxicity in cultured post-implantation rat embryos.	The Journal of Toxicological Sciences	39	285-292	2014
Usami M., Mitsunaga K., Miyajima A., Takamatu M., Kazama S., Irie T., Doi O., Takizawa T.	Effects of 13 developmentally toxic chemicals on the migration of rat cephalic neural crest cels in vitro.	Congenital Anomalies			2015
Irie T., Kikura-Hanajiri R., Usami M., Uchiyama N., Goda Y., Sekino Y	MAM-2201, a synthetic cannabinoid drug of abuse, suppresses the synaptic input to cerebellar Purkinje cells via activation of presynaptic CB1 receptors.	Neuropharmacology	95	479–91	2015
Oguchi-Katayama A., Monma A., Sekino Y., Moriguchi T., Sato K	Comparative gene expression analysis of the amygdalae of juvenile rats exposed to valproic acid at prenatal and postnatal stages.	J Toxicol Sci	38 (3)	381-402	2013
Takahashi K., Ishii-Nozawa R., Takeuchi K., Nakazawa K., Sekino Y., Sato K.	Niflumic acid activates additional currents of the human glial L-glutamate transporter EAAT1 in a substrate-dependent manner.	Biol Pharm Bull	36 (12)	1996-2004	2013
Fujimori, K., Takaki, J., Miura, M., Shigemoto-Mogami, Y., Sekino, Y., Suzuki, T., Sato, K.	Paroxetine prevented the down-regulation of astrocytic L-Glu transporters in neuroinflammation.	J Pharamcol Sci (in press)			
Shigemoto-Mogami, Y., Hoshikawa, K., Goldman, J.E.,Sekino, Y., Sato, K.	Microglia enhances neurogenesis and oligodendrogenesis in the early postnatal subventricular zone.	J Neurosci.	34(5)	2231-2243	2014
Shigemoto-Mogami, Y., Fujimori, K., Ikarashi, Y., Hirose, A., Sekino, Y., Sato, K.	Residual metals in carbon nanotubes suppress the proliferation of neural stem cells.	Fundam Toxcol Sci.	1(3)	87-94	2014
佐藤　薫	ミクログリアの発生と分化	Clinical Neuroscience	32 (12)	1338-1341	2015
Sato, K.	Microglia effects on neuronal development.	GLIA	63 (8)	1394-495	2015
吉田祥子・穂積直裕	神経伝達物質を視るデバイスが拓く神経科学の展開 ～ 求められる技術を開発する技術 ～	信学技報	112-345	39-40	2012
吉田祥子・穂積直裕	発達期小脳アストロサイトの機能と秩序形成	JNNS.	20	14-18	2013

K. Watanabe, N. Takahashi, N. Hozumi, S. Yoshida,	Improvements in Enzyme-Linked Photo assay Systems for Spatiotemporal Observation of Neurotransmitter Release	Sensors and Materials	27 (10)	1035–1044	2015
H. Mabuchi, HY Ong, K. Watanabe, S. Yoshida, N. Hozumi,	Visualization of Spatially Distributed Bioactive Molecules Using Enzyme-Linked Photo Assay	IEEJ Transactions (in press)			
上野　晋	化学物質（金属・有機溶剤）の毒性学と産業医としての対応	産業医科大学雑誌	第35巻特集号	91-6	2013
Park EK, Wilson D, Choi HJ, Wilson CT, Ueno S.	Hazardous metal pollution in the republic of Fiji and the need to elicit human exposure.	Environ Health Toxicol.			2013
Obara G., Toyohira Y., Inagaki H., Takahashi K., Horishita T., Kawasaki T., Ueno S., Tsutsui M., Sata T., Yanagihara N.	Pentazocine inhibits norepinephrine transporter function by reducing its surface expression in bovine adrenal medullary cells.	*J Pharmacol Sci.*	121	138-47	2013
Uchida T., Furuno Y., Tanimoto A., Toyohira Y., Arakaki K., Kina-Tanada M., Kubota H., Sakanashi M., Matsuzaki T., Noguchi K. Nakasone J., Igarashi T., Ueno S., Matsushita M., Ishiuchi S., Masuzaki H., Ohya Y., Yanagihara N., Shimokawa H., Otsuji Y., Tamura M., Tsutsui M.	Development of an experimentally useful model of acute myocardial infarction: 2/3 nephrectomized triple nitric oxide synthases-deficient mouse.	J Mol Cell Cardiol.	77	29-41	2014
Horishita T., Yanagihara N., Ueno S., Sudo Y., Uezono Y., Okura D., Minami T., Kawasaki T., Sata T.	Neurosteroids allopregnanolone sulfate and pregnanolone sulfate have diverse effect on the a subunit of the neuronal voltage-gated sodium channels Nav1.2, Nav1.6, Nav1.7, and Nav1.8 expressed in *Xenopus* oocytes.	Anesthesiology.	121	620-631	2014
Okura D., Horishita T., Ueno S., Yanagihara N., Sudo Y., Uezono Y., Sata T.	The endocannabinoid anandamide inhibits voltage-gated sodium channels Nav1.2, Nav1.6, Nav1.7 and Nav1.8 in Xenopus oocytes.	Anesth. Analg.	118	554-62	2014
Yanagihara N, Zhang H, Toyohira Y, Takahashi K, Ueno S, Tsutsui M, Takahashi K.	New insights into the pharmacological potential of plant flavonoids in the catecholamine system.	J Pharmacol Sci.	124	123-8	2014

Inagaki H, Toyohira Y, Takahashi K, Ueno S, Obara G, Kawagoe T, Tsutsui M, Hachisuga T, Yanagihara N.	Effects of selective estrogen receptor modulators on plasma membrane estrogen receptors and catecholamine synthesis and secretion in cultured bovine adrenal medullary cells.	J Pharmacol Sci.	124	66-75	2014
Okura D., Horishita T., Ueno S., Yanagihara N., Sudo Y., Uezono Y., Minami T., Kawasaki T., Sata T.	Lidocaine preferentially inhibits the function of purinergic P2X7 receptors expressed in *Xenopus* Oocytes.	Anesth Analg.	120	597-605	2015
Ishidao T, Fueta Y, Ueno S, Yoshida Y, Hori H.	A cross-fostering analysis of bromine ion concentration in rats that that inhaled 1-bromopropane vapor.	*J. Occup. Health*, in press.			
Fueta Y, Kanemitsu M, Egawa S, Ishidao T, Ueno S, Hori H.	Prenatal exposure to 1-bromopropane suppresses kainate-induced wet dog shakes in immature rats.	*J UOEH.*	37	255-261	2015
Li X, Toyohira Y, Horisita T, Satoh N, Takahashi K, Zhang H, Iinuma M, Yoshinaga Y, Ueno S, Tsutsui M, Sata T, Yanagihara N.	Ikarisoside A inhibits acetylcholine-induced catecholamine secretion and synthesis by suppressing nicotinic acetylcholine receptor-ion channels in cultured bovine adrenal medullary cells.	*Naunyn Schmiedebergs Arch Pharmacol*.	388	1259-1269	2015

書籍

著者氏名	論文タイトル名	書籍全体の編集者名	書　籍　名	出版社名	出版地	出版年	ページ
Kanda Y.	Assessment of cigarette smoking toxicity using cancer stem cells.	Nazmi Sari	Smoking Restrictions, Risk Perceptions and Its Health and Environmental Impacts	Nova Science Publishers	United States of America	2014	185-196
Kanda Y.	1. Cancer Stem Cells - Fact or Fiction?	Dittmar T, Zänker KS	Role of Cancer Stem Cells in Cancer Biology and Therapy	CRC Press	United States of America	2013	1-22
諫田泰成	ヒトiPS細胞を用いた心毒性試験の現状と課題	安全性評価研究会編集委員会	谷本学校毒性質問箱第16号	株式会社サイエンティスト社	東京	2014	91-94
諫田泰成	再生心筋細胞を用いた安全性薬理評価系の開発	エイブル株式会社和田昌憲	再生医療における臨床研究と製品開発	技術情報協会	東京	2013	572-576

The Journal of Toxicological Sciences (J. Toxicol. Sci.)
Vol.38, No.3, 513-521, 2013

Original Article

Involvement of decreased glutamate receptor subunit GluR2 expression in lead-induced neuronal cell death

Keishi Ishida[1], Yaichiro Kotake[1], Masatsugu Miyara[1], Kaori Aoki[1], Seigo Sanoh[1], Yasunari Kanda[2] and Shigeru Ohta[1]

[1]Graduate School of Biomedical and Health Sciences, Hiroshima University, 1-2-3 Kasumi, Minami-ku, 734-8553, Japan
[2]Division of Pharmacology, National Institute of Health Sciences, 1-18-1, Kamiyoga, Setagaya-ku 158-8501, Japan

(Received April 4, 2013; Accepted April 25, 2013)

ABSTRACT — Lead is known to induce neurotoxicity, particularly in young children, and GluR2, an AMPA-type glutamate receptor subunit, plays an important role in neuronal cell survival. Therefore, we hypothesized that altered GluR2 expression plays a role in lead-induced neuronal cell death. To test this idea, we investigated the effect of exposure to 5 and 20 μM lead for 1-9 days on the viability and GluR2 expression of primary-cultured rat cortical neurons. The number of trypan-blue stained cells was increased by exposure to 5 μM lead for 9 days or 20 μM lead for 7-9 days, and LDH release was increased after exposure to 20 μM lead for 9 days. GluR2 expression was reduced by exposure to 5-100 μM lead, but not 0.1-1 μM lead, for 9 days. Immunocytochemistry also confirmed that GluR2 expression was decreased in the presence of lead. Application of 50 ng/ml brain-derived neurotrophic factor (BDNF) led to a recovery of lead-induced neuronal cell death, accompanied with increased GluR2 expression. Our results suggest that long-term exposure to lead induces neuronal cell death, in association with a decrease of GluR2 expression.

Key words: Lead, GluR2, Brain-derived neurotrophic factor

INTRODUCTION

Lead has been widely used in many products; for example, leaded gasoline, lead-based paint, and cans containing foods or alcoholic beverages. Exposure to high levels of environmental lead causes various public health problems, particularly among young children, because of its effects on the blood and brain, including disruption of nervous system communication (Gracia and Snodgrass, 2007). Recently, regulation of industrial and environmental levels of lead has been strengthened in many countries, but soil and water contamination is a persistent source of lead exposure in industrialized societies. Toxicity typically results from ingestion of food or water contaminated with lead, but may also occur after accidental ingestion of contaminated dust, soil, or lead-containing paints (Gracia and Snodgrass, 2007). Over 90% of lead absorbed after inhalation or oral ingestion is retained in the body and distributed to the bones (Links *et al.*, 2001), where the half-life of lead is decades long. It was reported that individuals with baseline blood lead levels of 10 to 19 μg/dl suffer increased mortality from various causes: for example, mortality due to circulatory disease was increased by 10% and mortality due to cancer was increased by 46% relative to individuals with blood lead levels of less than to 10 μg/dl (Lustberg and Silbergeld, 2002). Thus, blood lead level is positively associated with mortality due to circulatory disorders and cancers.

Lead is known to induce neurotoxicity, leading to lowered intelligence test scores, behavioral problems and decreased cognitive ability (Canfield *et al.*, 2004; Laidlaw *et al.*, 2005). Lead-related intellectual deficits are seen in children with blood lead levels of at least 10 μg/dl, though no evidence of a threshold was found (Lanphear *et al.*, 2005). Schoolchildren with elevated blood lead levels due to both pre- and postnatal lead exposure are more likely to exhibit disruptive behavior in class (Leviton *et al.*, 1993; Bellinger *et al.*, 1994). Moreover, childhood exposure to lead is a risk factor for attention-deficit/hyperactivity disorder (ADHD) (Froehlich *et al.*,

Correspondence: Yaichiro Kotake (E-mail: yaichiro@hiroshima-u.ac.jp)

2009). However, the mechanisms involved have not been clarified in detail.

Glutamate is an essential amino acid in the central nervous system. Glutamate receptors affect the survival and maturation of cortical, mesencephalic, and cerebellar granule neurons (Blandini *et al.*, 1996; Monti *et al.*, 2002; Hirasawa *et al.*, 2003), and play a central role in learning and memory. Ca^{2+} influx through glutamate receptors due to excitotoxic and ischemic damage can trigger multiple intracellular cascades and cause damage to neuronal cells in the brain (Choi, 1988; Tymianski, 1996; Ying *et al.*, 1997). Ionotropic glutamate receptors are mainly divided into two types, *N*-methyl-D-aspartate (NMDA) receptors and α-amino-3-hydroxy-5-methylisoxazole-4-propionic acid (AMPA) receptors. NMDA receptors are composed of an obligatory NR1 subunit and accessory subunits from the NR2 or NR3 family and the latter subunits are expressed differentially during development. Each subunit plays a specific role, contributing to the subcellular localization and channel properties of NMDA receptors (Luo *et al.*, 2011). Thus, changes of NMDA receptor subunit composition influence neuronal activity and survival. On the other hand, AMPA receptors are heteromeric complexes composed of four subunits (GluR1 to GluR4). Among the AMPA receptor subunits, GluR2 is expressed widely in hippocampal pyramidal and granule neurons (Hollmann and Heinemann, 1994) and in cortical neurons (Kondo *et al.*, 1997). AMPA receptor channel impermeability to Ca^{2+} is dependent upon the GluR2 subunit, and cells that contain AMPA receptor lacking the GluR2 subunit show high Ca^{2+} permeability and vulnerability to excitotoxicity (Liu and Zukin, 2007).

Lead is a potent, non-competitive and voltage-independent antagonist of NMDA receptor (Alkondon *et al.*, 1989). It is reported that lead binding at the Zn^{2+}-binding site of NMDA receptor is dependent on the receptor composition, i.e., lead showed competitive inhibition at the Zn^{2+} binding site of NR2A, but not at the Zn^{2+} binding site of NR2B (Gavazzo *et al.*, 2008). Moreover, lead alters NMDA receptor subunit composition. Expression of NR2A and NR1 is decreased (Nihei *et al.*, 2000) and the expression of NR1 splice variant mRNA is altered (Guilarte *et al.*, 2000) in rat hippocampus following exposure to lead. Further, lead exposure during synaptogenesis changes NMDA receptor expression at developing synapses (Neal *et al.*, 2011). Thus, lead-induced changes of NMDA receptor subunit composition may result in disruption of downstream signaling. However, the effects of lead on AMPA receptors have not been investigated. Therefore, in the present work, we investigated the effect of lead on the viability and GluR2 expression of primary-cultured rat cortical neurons to test our hypothesis that decreased GluR2 expression is involved in lead-induced neuronal cell death.

MATERIALS AND METHODS

Materials

Eagle's minimal essential salt medium (Eagle's MEM) was purchased from Nissui Pharmaceutical (Tokyo, Japan). Fetal calf serum (FCS) was purchased from Nichirei Biosciences Inc. (Tokyo, Japan). Horse serum (HS) was purchased from Gibco (Life Technologies, Carlsbad, CA, USA). Trypan blue, D-(+)-glucose, $NaHCO_3$, sodium orthovanadate, phenylmethylsulfonyl fluoride (PMSF), sodium dodecyl sulfate (SDS), glycerol, and paraformaldehyde were purchased from Wako (Tokyo, Japan). Lead acetate was purchased from EBISU (Osaka, Japan). HEPES was purchased from DOJINDO (Kumamoto, Japan). L-Glutamine, arabinocylcytosine, formaldehyde and anti-β-actin antibody (AC-15) were purchased from Sigma-Aldrich (St. Louis, MO, USA). Pentobarbital was purchased from Kyoritsu (Tokyo, Japan). Bromophenol blue was purchased from Katayama Chemical Industries Co., Ltd. (Osaka, Japan). Tris-HCl, nonidet P-40, EDTA, mercaptoethanol and Protease Inhibitor Cocktail was purchased from Nacalai Tesque (Kyoto, Japan). Anti-GluR2 antibody (MAB397) was purchased from Millipore (Billerica, MA, USA). Anti-N-cadherin antibody (sc-7939) was purchased from Santa Cruz Biotechnology (Dallas, TX, USA).

Cell culture

The following procedures were performed under sterile conditions. The present study was approved by the university's animal ethics committee of Hiroshima University. Primary cultures were obtained from cerebral cortex of fetal rats at 18 days of gestation. Fetuses were taken from pregnant Slc:Wistar/ST rats under pentobarbital anesthesia. The prefrontal part of the cerebral cortex was dissected with a razor blade, and cells were dissociated by gentle pipetting. Dissociated cells were plated on culture plates (4×10^5 cells/cm^2). Cultures were incubated in Eagle's MEM supplemented with 10% heat-inactivated FCS, L-glutamine (2 mM), D-(+)-glucose (11 mM), $NaHCO_3$ (24 mM), and HEPES (10 mM). Cultures were maintained at 37°C in an atmosphere of humidified 5% CO_2 in air. The cultures were incubated in MEM containing 10% FCS (days *in vitro* (DIV) 1-7) or 10% HS (DIV 8-11). The medium was exchanged every 2 days. Arabinocylcytosine (10 μM) was added to inhibit the proliferation of non-neuronal cells after DIV 6. Cultures were

used for experiments at DIV 11. This protocol has been confirmed to produce cultures containing about 90% neurons by immunostaining for a neuron marker MAP2.

Treatment of cultures

Medium containing lead was changed at DIV 2, 4, 6, 8, and 10 and the neurons were exposed until DIV 11 for 9 days. In BDNF experiment, BDNF was added to the culture medium at DIV 2 and further added every day until DIV 10. Thus, the neurons were exposed also with BDNF for 9 days.

Trypan blue assay

After exposure to lead acetate, cell cultures were stained with 1.5% trypan blue for 10 min, then fixed with 10% formalin for 2 min, and rinsed with physiological saline. Unstained cells were regarded as viable and stained cells were regarded as dead. The viability of the cultures was calculated as the percentage ratio of the number of unstained cells to the total cells counted. Over 200 cells per cover slip were randomly counted.

LDH assay

LDH release was measured using a CytoTox 96 Non-Radioactive Cytotoxicity Assay (Promega®) according to the manufacturer's protocol. After exposure to lead acetate, culture medium (50 μl) was transferred to a 96-well plate. Substrate mixture (50 μl) was added to each well and allowed to react for 30 min in the dark at room temperature. Stop solution (50 μl) was then added to each well, and the absorbance was read at 490 nm. The absorbance was normalized based on the absorbance of negative controls, which consisted of cells not exposed to lead.

Western blotting

After lead acetate treatment, cells were washed with PBS buffer and lysed in TNE buffer containing 50 mM Tris-HCl, 1% nonidet P-40, 20 mM EDTA, Protease Inhibitor Cocktail (1:200), 1 mM sodium orthovanadate, and 1 mM PMSF. The mixture was rotated at 4°C and centrifuged at 15,000 rpm, after which the supernatant was transferred to a microtube. The supernatant was added to sample buffer containing 100 mM Tris-HCl, 4% SDS, 20% glycerol, 0.004% bromophenol blue, and 5% mercaptoethanol, and then denatured at 95°C for 3 min. Protein was separated by SDS-polyacrylamide gel electrophoresis and transferred to a polyvinylidene difluoride membrane. The membrane was blocked with blocking buffer containing 5% skim milk for 1 hr, and then incubated with anti-GluR2 (1:2,000) and anti-β-actin (1:4,000) overnight, and with secondary antibody for 1 hr. Other details were performed by the methods described previously (Hashida *et al.*, 2011). The protein was detected with an enhanced chemiluminescence detection system (Chemi-Lumi One L, Nacalai Tesque (Kyoto, Japan)). Quantitative analysis was performed with digital imaging software (Image J, NIH (Bethesda, MD, USA)), and GluR2 protein levels were corrected on the basis of β-actin protein levels.

Immunocytochemistry

Cells were seeded in poly-D-lysine-coated 8-well chamber slides (BD BioCoat™) and incubated overnight. After treatment with 5 and 20 μM lead for 9 days, cells were washed with PBS(-) and fixed with 4% paraformaldehyde in PBS(-) for 15 min at room temperature. The slides were washed with PBS(-), blocked with 4 drops of Image-iT™ FX Signal Enhancer (Molecular Probes®) for 1 hr, and incubated with mouse anti-GluR2 (MAB397), which recognizes the N-terminal extracellular domain of GluR2 (1:250), and rabbit anti-N-cadherin (1:250) diluted in PBS(-) overnight at 4°C. Then, the slides were washed three times with PBS(-), and incubated with Alexa Fluor® 488-conjugated goat anti-mouse IgG (1:800, Molecular Probes®) and Alexa Fluor® 555-conjugated goat anti-rabbit IgG (1:800, Molecular Probes®) for 1 hr at room temperature in the dark. The slides were further washed three times with PBS(-), incubated with 4',6-diamidino-2-phenylindole dihydrochloride (DAPI, 1:2,000, Molecular Probes®) diluted in PBS(-) for 5 min, and washed again three times with PBS(-). Finally, the slides were enclosed in Prolong® Gold (Molecular Probes®) and observed under a confocal laser scanning microscope (Olympus, FV-1000-D).

Statistics

All the experiments were performed at least three times and representative data are shown. Data are expressed as mean + S.E.M. Statistical evaluation of the data was performed with ANOVA followed by Tukey's test. A value of $P < 0.05$ was considered to be indicative of significance.

RESULTS

Lead-induced cell death of cortical neurons

First, we investigated neuronal cell death induced by long-term exposure to lead. Rat cortical neurons were exposed to 5 and 20 μM lead for 1, 3, 5, 7, and 9 days, and then the cell viability was examined by means of trypan blue assay (Fig. 1A) and LDH assay (Fig. 1B). Exposure of the cells to 5 μM lead for 9 days resulted in a decrease of the cell viability to 29% of the control, while

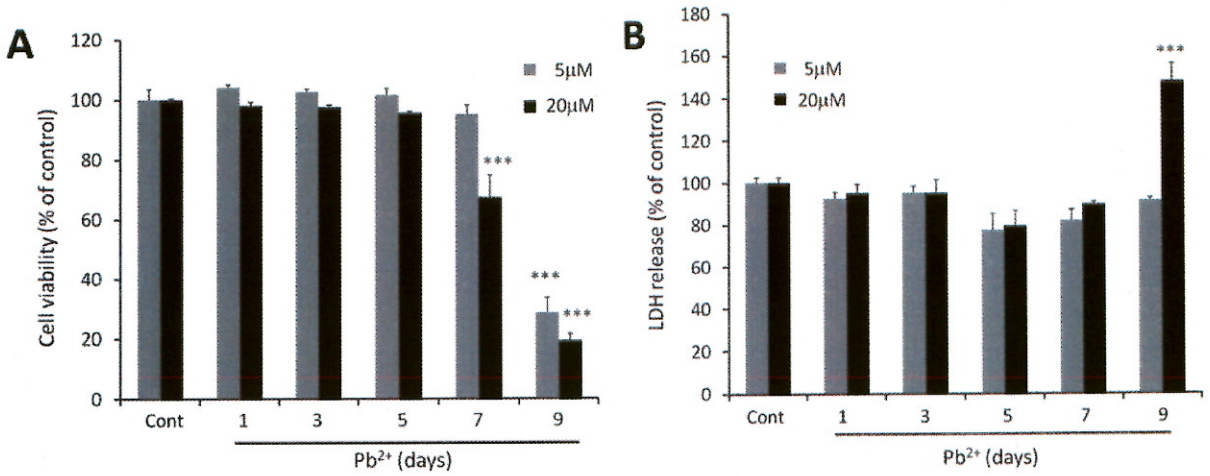

Fig. 1. Influence of long-term exposure to lead acetate (Pb^{2+}) on neurotoxicity. Cortical neurons were exposed to 5 and 20 μM Pb^{2+} for 1-9 days. Then cell viability was measured by means of trypan blue assay (A) and LDH assay (B). Data are expressed as mean + S.E.M. (n = 4). ***P < 0.001 vs. Cont.

exposure to 20 μM lead for 7 and 9 days decreased the cell viability to 67% and 19% of the control, respectively (Fig. 1A). Moreover, LDH release from cortical neurons was increased to 147% of the control after exposure to 20 μM lead for 9 days, although exposure to 5 μM lead had no effect (Fig. 1B).

Effect of long-term exposure of lead on GluR2 expression

We hypothesized that long-term exposure to lead would also decrease GluR2 expression, and would result in neuronal cell death. To examine this hypothesis, cortical neurons were exposed to 0.1-100 μM lead for 9 days and GluR2 protein expression was measured. As shown in Fig. 2A, a concentration-dependent decrease of GluR2 expression was seen upon exposure of the neurons to lead at concentrations above 1 μM and the decrease reached statistical significance at 5 μM. In 100 μM lead exposure, β-actin expression was also decreased, maybe due to drastic cell death (Fig. 2A). Moreover, cortical neurons were exposed to 5 and 20 μM lead for 1-9 days. A time-dependent decrease of GluR2 expression was observed in the neurons exposed to 5 and 20 μM lead. Exposure to 5 μM lead for 7 and 9 days significantly decreased the expression of GluR2 to 50% and 29% of the control (Fig. 2B), while exposure to 20 μM lead for 7 and 9 days significantly decreased the expression of GluR2 to 35% and 30% of the control (Fig. 2C). GluR2 subunits are largely expressed in cytoplasm, but some of them are expressed in plasma membrane and act as components of AMPA receptors. Next, GluR2 expression at the plasma membrane was examined by immunocytochemistry (Fig. 3). Membrane expression of GluR2, which was confirmed by co-localization with N-cadherin, a membrane protein marker, was observed in the control cells. Exposure to 5 and 20 μM lead for 9 days markedly decreased GluR2 expression, in accordance with the result of western blotting (Fig. 2). Moreover, co-localization of GluR2 and N-cadherin was also considerably reduced, while intracellular distribution of GluR2 was not altered in these cells. These results suggest that exposure to lead decreases GluR2 expression, leading to a decrease in plasma membrane GluR2.

Amelioration of lead-induced GluR2 reduction and neuronal cell death by BDNF

It has been reported that BDNF potently induces GluR2 promoter activity in SH-SY5Y cells, resulting in increased expression of GluR2 protein (Brené *et al.*, 2000). Thus, we tested whether BDNF also increased GluR2 protein expression in cortical neurons and ameliorated lead-induced neuronal cell death. Although the GluR2 protein level was not increased, the decrease of GluR2 expression induced by exposure to 5 and 20 μM lead was partly reversed by 50 ng/ml BDNF (Fig. 4A). Concomitantly, the decrease of cell viability caused by exposure to 5 and 20 μM lead was also significantly ameliorated by 50 ng/ml BDNF (Fig. 4B).

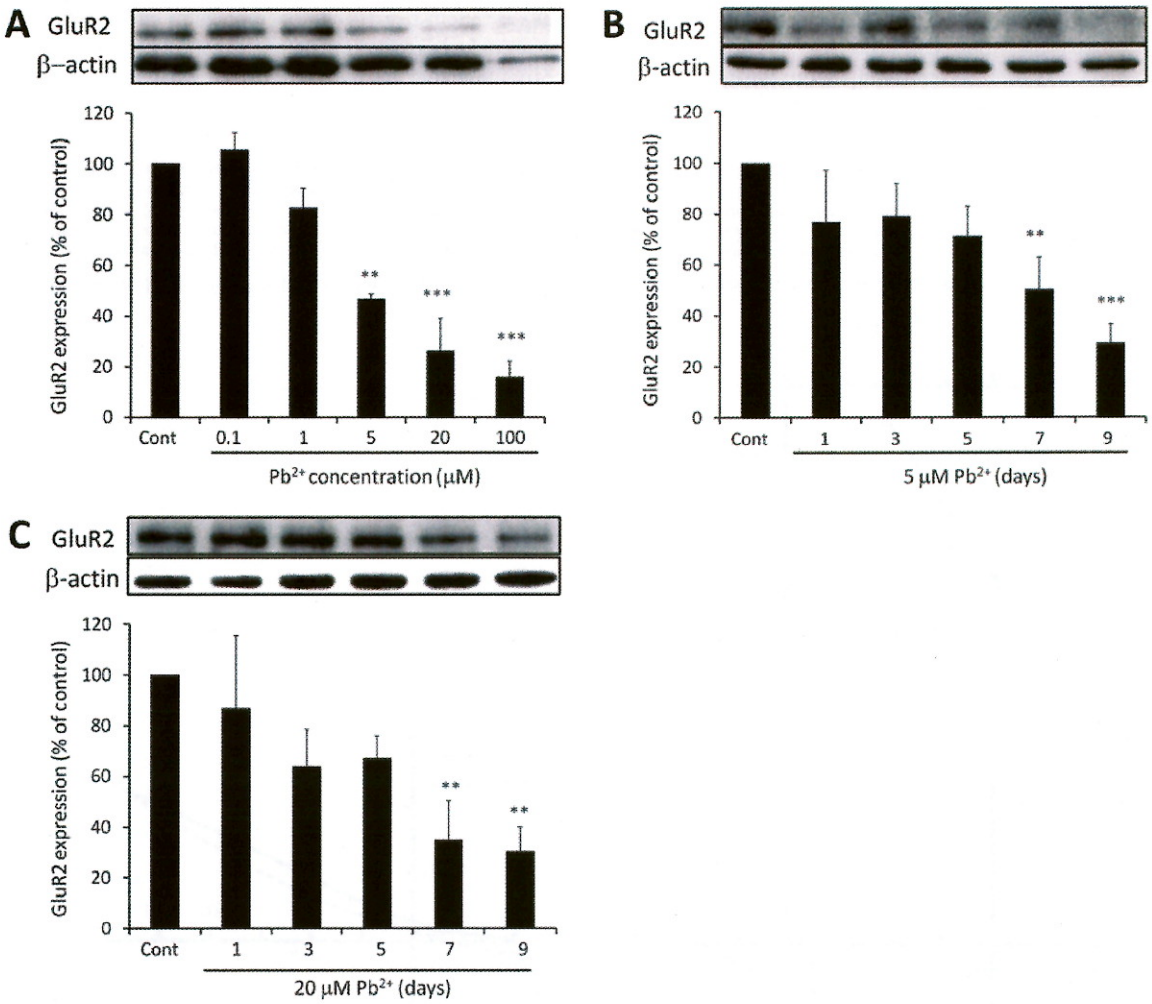

Fig. 2. Change of GluR2 protein expression induced by Pb^{2+}. Cortical neurons were exposed to 0.1-100 μM Pb^{2+} for 9 days (A), 5 μM Pb^{2+} for 1-9 days (B) and 20 μM (C) Pb^{2+} for 1-9 days, then GluR2 protein was detected by western blotting. Quantitative analysis was performed with Image J software and GluR2 protein levels were corrected on the basis of β-actin protein levels. Data are expressed as mean + S.E.M. (n = 3) **P < 0.01 vs. cont, ***P < 0.001 vs. cont.

DISCUSSION

In this study, cultured rat cortical neurons were exposed to lead to test our hypothesis that lead induces a decrease of GluR2 expression that in turn promotes neuronal cell death. We found that exposure to lead at 5-20 μM for 9 days decreased cell viability (Fig. 1A) and LDH release was increased after exposure to 20 μM lead for 9 days (Fig. 1B). Trypan blue-stained cells are regarded as dead, whereas LDH assay measures LDH release from membrane-disrupted cells. Thus, the differences in evaluation of neuronal cell death between trypan blue assay and LDH assay is considered to be due to the different endpoints used to determine cell death in the two assays.

The expression of GluR2, an AMPA-type glutamate receptor subunit, was significantly decreased by exposure to 5-20 μM lead for 7 days (Fig. 2). It was reported that exposure to 0.1-10 μM lead for 48 hr decreased cell proliferation and increased caspase-3 activity in human SH-SY5Y neuroblastoma cells (Chetty *et al.*, 2005). Shinkai *et al.* (2010) reported that 5 μM lead induces endoplasmic

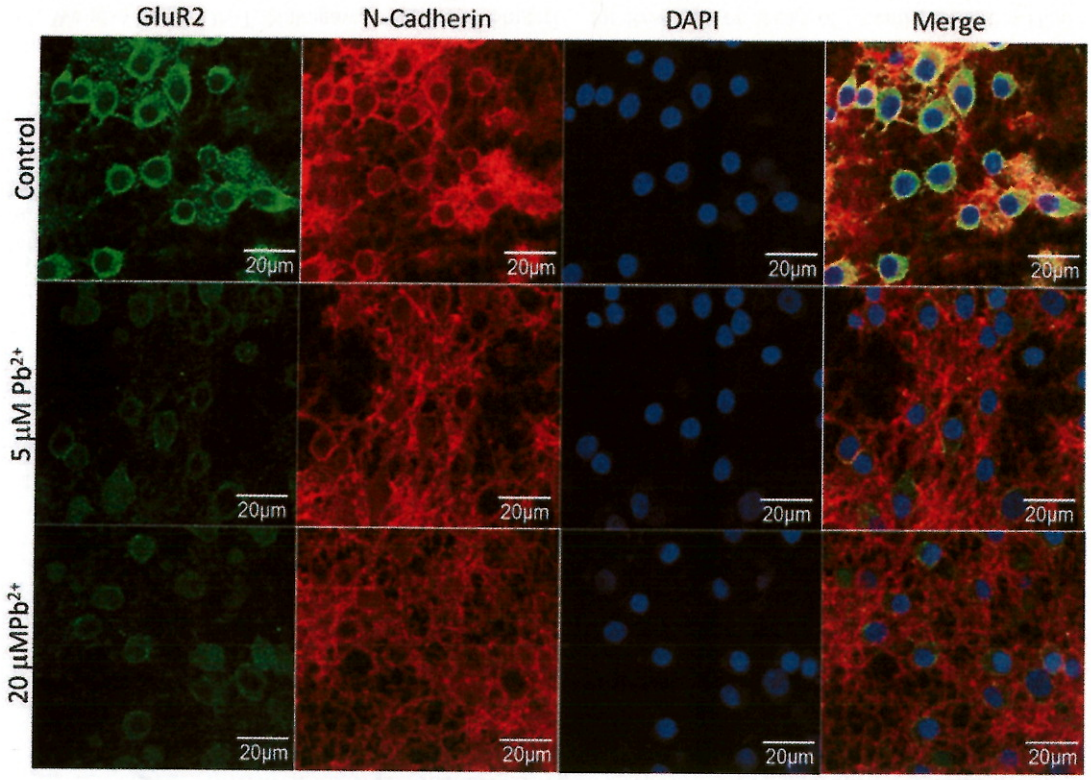

Fig. 3. Change of GluR2 protein expression on the plasma membrane induced by Pb^{2+}. Cortical neurons were exposed to 5 and 20 μM Pb^{2+} for 9 days, and immunocytochemical staining was performed using a mouse anti-GluR2 antibody that recognizes the N-terminal extracellular domain of GluR2 (green) and a rabbit anti-N-cadherin antibody (red). Nuclear staining was performed using DAPI (blue). Yellow indicates colocalization between GluR2 and N-cadherin.

reticulum chaperones GRP78 and GRP94 via JNK-AP-1 pathway in vascular endothelial cells. Thus, the lead concentrations used in this study are similar to those used in other studies on the *in vitro* toxicities of lead. Incidentally, lead concentrations of up to 5 μM in blood have been reported in workers exposed to lead (Tomokuni *et al.*, 1993). It is well known that lead induces hematotoxicity by inhibiting the activity of enzymes involved in heme biosynthesis such as δ-aminolevulinic acid dehydratase. It is believed to be the most sensitive to lead (Bottomley and Muller-Eberhard, 1988). However, δ-aminolevulinic acid dehydratase is inhibited only in the presence of comparatively high lead concentrations of 0.1-1 mM in human erythroblastic cultures (Rio *et al.*, 2001). Thus, the concentrations used in this study are lower than those used in the above studies.

We have reported that long-term exposure of rat cortical neurons to tributyltin (TBT) decreases GluR2 expression, which results in increased Ca^{2+} permeability of AMPA receptors, because the Ca^{2+} permeability of AMPA receptors depends on whether or not they contain the GluR2 subunit (Nakatsu *et al.*, 2009). It was reported that GluR2 knockdown rats showed neuronal cell death in hippocampal CA1 and CA3, and the neuronal cell death was reduced by injection of Naspm (an open channel blocker selective for Ca^{2+}-permeable, GluR2-lacking AMPA receptors) and CNQX (a competitive blocker of AMPA receptors) (Oguro *et al.*, 1999), which suggests that GluR2 knockdown-induced neuronal cell death was mediated by Ca^{2+}-permeable, GluR2-lacking AMPA receptors. It has also been reported that knockdown of GluR2 exacerbates kainate-induced neuronal death (Friedman and Velísková, 1998; Friedman *et al.*, 2003). Iihara *et al.* (2001) suggested that kainate-induced neuronal cell death in GluR2 knockdown animals involves altered Na^{2+} permeability as well as altered Ca^{2+} permeability. It

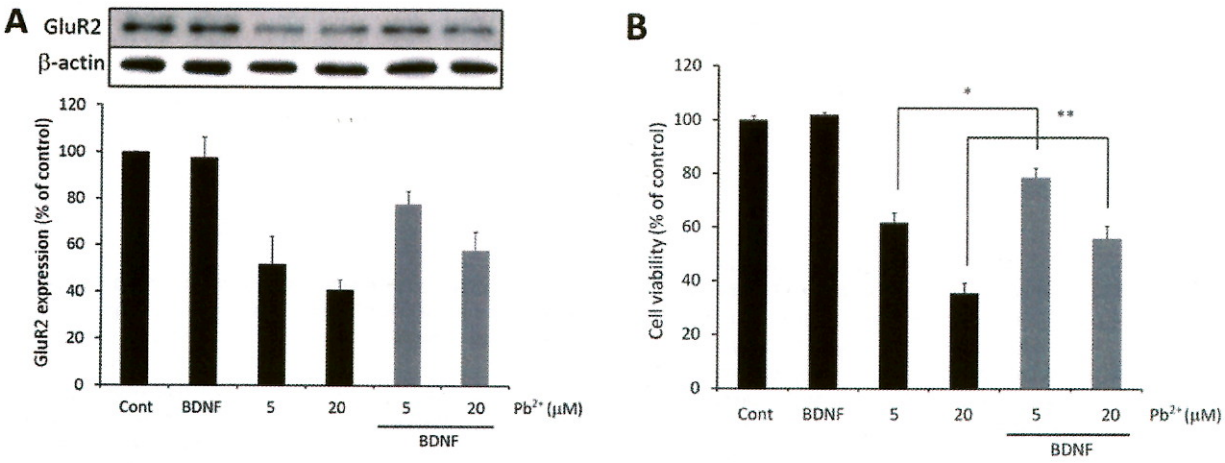

Fig. 4. Influence of exposure to BDNF on Pb^{2+}-induced decrease of GluR2 and neuronal cell death. Cortical neurons were exposed to 5 and 20 μM Pb^{2+} with or without 50 ng/ml BDNF for 9 days. (A) GluR2 protein was detected by western blotting. Quantitative analysis was performed with Image J software and GluR2 protein levels were corrected on the basis of β-actin protein levels. Data are expressed as mean + S.E.M. (n = 4-5). (B) Cell viability was measured by means of trypan blue assay. Data are expressed as mean + S.E.M. (n = 8). *P < 0.05, **P < 0.01.

is known that GluR2 knockdown mice also show behavioral changes, such as impaired novelty-induced exploratory activities, disrupted motor coordination, and reduced self-directed behaviors, compared with control mice (Jia *et al.*, 1996). These findings are consistent with the idea that lead-induced GluR2 decrease can induce neuronal death via the increase of Ca^{2+} permeability of AMPA receptors. However, further studies are needed to measure lead-induced Ca^{2+} entry into neurons.

Expression of GluR2 can be induced by BDNF (Brené *et al.*, 2000), and one of the neuroprotective effects of BDNF is supposed to be mediated by recovery of GluR2. We also investigated whether increasing GluR2 expression by exposure to BDNF results in amelioration of lead-induced neuronal cell death. We found that the lead-induced GluR2 decrease was partly reversed and neuronal cell viability was increased by exposure to 50 ng/ml BDNF (Fig. 4). Because GluR2 levels are thought to reach plateau in primary cortical neurons, BDNF may not increase basal GluR2 expression. These results support the hypothesis that lead causes neuronal cell death through decreasing GluR2 protein expression, though BDNF might rescue lead-induced neuronal death by other mechanism such as an activation of PI3-kinase-Akt pathway (Hetman *et al.*, 1999). It should be confirmed that GluR2 overexpression recovers cell viability decreased by lead.

In conclusion, we investigated the influence of long-term lead exposure on cultured cortical neurons. Lead induced a decrease of GluR2 protein and caused neuronal cell death. The decrease of GluR2 expression was considered to cause the lead-induced neuronal cell death, because cell viability was restored by BDNF treatment, which elicits a recovery of GluR2. A decrease in the population of GluR2-containing AMPA receptors is associated with increased Ca^{2+} influx. Our findings raise the possibility that GluR2 decrease in the brain is involved in lead-induced *in vivo* neurotoxicity, disorder of behavior, and impairment of cognitive function.

ACKNOWLEDGMENT

We thank the Analysis Center of Life Science, Hiroshima University for the use of their facilities. This work was supported by JSPS KAKENHI Grant Number 23310047 (to Y. Kotake).

REFERENCES

Alkondon, M., Costa, A.C., Radhakrishnan, V., Aronstam, R.S. and Albuquerque, E.X. (1990): Selective blockade of NMDA-activated channel currents may be implicated in learning deficits caused by lead. FEBS Lett., **261**, 124-130.

Bellinger, D., Leviton, A., Allred, E. and Rabinowitz, M. (1994): Pre- and postnatal lead exposure and behavior problems in school-aged children. Environ. Res., **66**, 12-30.

Blandini, F., Porter, R.H. and Greenamyre, J.T. (1996): Glutamate

and Parkinson's disease. Mol. Neurobiol., **12**, 73-94.
Bottomley, S.S. and Muller-Eberhard, U. (1988): Pathophysiology of heme synthesis. Semin. Hematol., **25**, 282-302.
Brené, S., Messer, C., Okado, H., Hartley, M., Heinemann, S.F. and Nestler, E.J. (2000): Regulation of GluR2 promoter activity by neurotrophic factors via a neuron-restrictive silencer element. Eur. J. Neurosci., **12**, 1525-1533.
Canfield, R.L., Gendle, M.H. and Cory-Slechta, D.A. (2004): Impaired neuropsychological functioning in lead-exposed children. Dev. Neuropsychol., **26**, 513-540.
Chetty, C.S., Vemuri, M.C., Campbell, K. and Suresh, C. (2005): Lead-induced cell death of human neuroblastoma cells involves GSH deprivation. Cell. Mol. Biol. Lett., **10**, 413-423.
Choi, D.W. (1988): Calcium-mediated neurotoxicity: relationship to specific channel types and role in ischemic damage. Trends Neurosci., **11**, 465-469.
Friedman, L.K., Segal, M. and Velísková, J. (2003): GluR2 knockdown reveals a dissociation between [Ca2+]i surge and neurotoxicity. Neurochem. Int., **43**, 179-189.
Friedman, L.K. and Velísková, J. (1998): GluR2 hippocampal knockdown reveals developmental regulation of epileptogenicity and neurodegeneration. Brain Res. Mol. Brain Res., **61**, 224-231.
Froehlich, T.E., Lanphear, B.P., Auinger, P., Hornung, R., Epstein, J.N., Braun, J. and Kahn, R.S. (2009): Association of tobacco and lead exposures with attention-deficit/hyperactivity disorder. Pediatrics, **124**, e1054-e1063.
Gavazzo, P., Zanardi, I., Baranowska-Bosiacka, I. and Marchetti, C. (2008): Molecular determinants of Pb2+ interaction with NMDA receptor channels. Neurochem. Int., **52**, 329-337.
Gracia, R.C. and Snodgrass, W.R. (2007): Lead toxicity and chelation therapy. Am. J. Health Syst. Pharm., **64**, 45-53.
Guilarte, T.R., McGlothan, J.L. and Nihei, M.K. (2000): Hippocampal expression of N-methyl-D-aspartate receptor (NMDAR1) subunit splice variant mRNA is altered by developmental exposure to Pb(2+). Brain Res. Mol. Brain Res., **76**, 299-305.
Hashida, T., Kotake, Y. and Ohta, S. (2011): Protein disulfide isomerase knockdown-induced cell death is cell-line-dependent and involves apoptosis in MCF-7 cells. J. Toxicol. Sci., **36**, 1-7.
Hetman, M., Kanning, K., Cavanaugh, J.E. and Xia, Z. (1999): Neuroprotection by brain-derived neurotrophic factor is mediated by extracellular signal-regulated kinase and phosphatidylinositol 3-kinase. J. Biol. Chem., **274**, 22569-22580.
Hirasawa, T., Wada, H., Kohsaka, S. and Uchino, S. (2003): Inhibition of NMDA receptors induces delayed neuronal maturation and sustained proliferation of progenitor cells during neocortical development. J. Neurosci. Res., **74**, 676-687.
Hollmann, M. and Heinemann, S. (1994): Cloned glutamate receptors. Annu. Rev. Neurosci., **17**, 31-108.
Iihara, K., Joo, D.T., Henderson, J., Sattler, R., Taverna, F.A., Lourensen, S., Orser, B.A., Roder, J.C. and Tymianski, M. (2001): The influence of glutamate receptor 2 expression on excitotoxicity in Glur2 null mutant mice. J. Neurosci., **21**, 2224-2239.
Jia, Z., Agopyan, N., Miu, P., Xiong, Z., Henderson, J., Gerlai, R., Taverna, F.A., Velumian, A., MacDonald, J., Carlen, P., Abramow-Newerly, W. and Roder, J. (1996): Enhanced LTP in mice deficient in the AMPA receptor GluR2. Neuron, **17**, 945-956.
Kjøller, C. and Diemer, N.H. (2000): GluR2 protein synthesis and metabolism in rat hippocampus following transient ischemia and ischemic tolerance induction. Neurochem. Int., **37**, 7-15.
Kondo, M., Sumino, R. and Okado, H. (1997): Combinations of AMPA receptor subunit expression in individual cortical neurons correlate with expression of specific calcium-binding proteins. J. Neurosci., **17**, 1570-1581.
Laidlaw, M.A., Mielke, H.W., Filippelli, G.M., Johnson, D.L. and Gonzales, C.R. (2005): Seasonality and children's blood lead levels: developing a predictive model using climatic variables and blood lead data from Indianapolis, Indiana, Syracuse, New York, and New Orleans, Louisiana (USA). Environ. Health Perspect., **113**, 793-800.
Lanphear, B.P., Hornung, R., Khoury, J., Yolton, K., Baghurst, P., Bellinger, D.C., Canfield, R.L., Dietrich, K.N., Bornschein, R., Greene, T., Rothenberg, S.J., Needleman, H.L., Schnaas, L., Wasserman, G., Graziano, J. and Roberts R. (2005): Low-level environmental lead exposure and children's intellectual function: an international pooled analysis. Environ. Health Perspect., **113**, 894-899.
Leviton, A., Bellinger, D., Allred, E.N., Rabinowitz, M., Needleman, H. and Schoenbaum, S. (1993): Pre- and postnatal low-level lead exposure and children's dysfunction in school. Environ. Res., **60**, 30-43.
Links, J.M., Schwartz, B.S., Simon, D., Bandeen-Roche, K. and Stewart, W.F. (2001): Characterization of toxicokinetics and toxicodynamics with linear systems theory: application to lead-associated cognitive decline. Environ. Health Perspect., **109**, 361-368.
Liu, S.J. and Zukin, R.S. (2007): Ca2+-permeable AMPA receptors in synaptic plasticity and neuronal death. Trends Neurosci., **30**, 126-134.
Luo, T., Wu, W.H. and Chen, B.S. (2011): NMDA receptor signaling: death or survival? Front Biol., **6**, 468-476.
Lustberg, M. and Silbergeld, E. (2002): Blood lead levels and mortality. Arch. Intern. Med., **162**, 2443-2449.
Monti, B., Marri, L. and Contestabile, A. (2002): NMDA receptor-dependent CREB activation in survival of cerebellar granule cells during *in vivo* and *in vitro* development. Eur. J. Neurosci., **16**, 1490-1498.
Nakatsu, Y., Kotake, Y., Takishita, T. and Ohta, S. (2009): Long-term exposure to endogenous levels of tributyltin decreases GluR2 expression and increases neuronal vulnerability to glutamate. Toxicol. Appl. Pharmacol., **240**, 292-298.
Neal, A.P., Worley, P.F. and Guilarte, T.R. (2011): Lead exposure during synaptogenesis alters NMDA receptor targeting via NMDA receptor inhibition. Neurotoxicology, **32**, 281-289.
Nihei, M.K., Desmond, N.L., McGlothan, J.L., Kuhlmann, A.C. and Guilarte, T.R. (2000): N-methyl-D-aspartate receptor subunit changes are associated with lead-induced deficits of long-term potentiation and spatial learning. Neuroscience, **99**, 233-242.
Oguro, K., Oguro, N., Kojima, T., Grooms, S.Y., Calderone, A., Zheng, X., Bennett, M.V. and Zukin, R.S. (1999): Knockdown of AMPA receptor GluR2 expression causes delayed neurodegeneration and increases damage by sublethal ischemia in hippocampal CA1 and CA3 neurons. J. Neurosci., **19**, 9218-9227.
Rio, B., Froquet, R. and Parent-Massin, D. (2001): In vitro effect of lead acetate on human erythropoietic progenitors. Cell. Biol. Toxicol., **17**, 41-50.
Shinkai, Y., Yamamoto, C. and Kaji, T. (2010): Lead induces the expression of endoplasmic reticulum chaperones GRP78 and GRP94 in vascular endothelial cells via the JNK-AP-1 pathway. Toxicol. Sci., **114**, 378-386.
Tomokuni, K., Ichiba, M. and Fujishiro, K. (1993): Interrelation between urinary delta-aminolevulinic acid (ALA), serum ALA,

and blood lead in workers exposed to lead. Ind. Health, **31**, 51-57.

Tymianski, M. (1996): Cytosolic calcium concentrations and cell death *in vitro*. Adv. Neurol., **71**, 85-105.

Ying, H.S., Weishaupt, J.H., Grabb, M., Canzoniero, L.M., Sensi, S.L., Sheline, C.T., Monyer, H. and Choi, D.W. (1997): Sublethal oxygen-glucose deprivation alters hippocampal neuronal AMPA receptor expression and vulnerability to kainate-induced death. J. Neurosci., **17**, 9536-9544.

Metallomics

RSC Publishing

PAPER

AMP-activated protein kinase-mediated glucose transport as a novel target of tributyltin in human embryonic carcinoma cells†

Cite this: DOI: 10.1039/c3mt20268b

Shigeru Yamada,[a] Yaichiro Kotake,[b] Yuko Sekino[a] and Yasunari Kanda*[a]

Received 28th December 2012,
Accepted 20th February 2013

DOI: 10.1039/c3mt20268b

www.rsc.org/metallomics

Organotin compounds such as tributyltin (TBT) are known to cause various forms of cytotoxicity, including developmental toxicity and neurotoxicity. However, the molecular target of the toxicity induced by nanomolar levels of TBT has not been identified. In the present study, we found that exposure to 100 nM TBT induced growth arrest in human pluripotent embryonic carcinoma cell line NT2/D1. Since glucose provides metabolic energy, we focused on the glycolytic system. We found that exposure to TBT reduced the levels of both glucose-6-phosphate and fructose-6-phosphate. To investigate the effect of TBT exposure on glycolysis, we examined glucose transporter (GLUT) activity. TBT exposure inhibited glucose uptake *via* a decrease in the level of cell surface-bound GLUT1. Furthermore, we examined the effect of AMP-activated protein kinase (AMPK), which is known to regulate glucose transport by facilitating GLUT translocation. Treatment with the potent AMPK activator, AICAR, restored the TBT-induced reduction in cell surface-bound GLUT1 and glucose uptake. In conclusion, these results suggest that exposure to nanomolar levels of TBT causes growth arrest by targeting glycolytic systems in human embryonic carcinoma cells. Thus, understanding the energy metabolism may provide new insights into the mechanisms of metal-induced cytotoxicity.

Introduction

Growing evidence suggests that environmental metals contribute to developmental toxicity and neurotoxicity.[1–3] Since the developing brain is inherently more vulnerable to injury than the adult brain, exposure to metals during early fetal development can potentially cause neurological disorders at doses much lower than those that are toxic in adults.[4–7] Therefore, it is necessary to elucidate the cytotoxic effects of such metals at low levels.

Organotin compounds are well known to cause cytotoxicity. Although organotin compounds or derivatives have been shown to have a potential anti-tumor activity[8,9] and some of them have already been entered into preclinical trials,[10] tributyltin (TBT) is considered to be associated with developmental toxicity and neurotoxicity.[11] For example, TBT can cause increased fetal mortality, decreased fetal birth weights, and behavioral abnormalities in rat offspring.[12,13] TBT is known to affect fertilization and embryonic development.[14] Moreover, TBT has been shown to induce neuronal death by glutamate excitotoxicity in cultured rat cortical neurons.[15] Although the use of TBT has already been restricted, butyltin compounds, including TBT, have been reported to be still present at concentrations between 50 and 400 nM in human blood.[16] However, the mechanism by which nanomolar levels of TBT cause cytotoxicity is not fully understood.

Glucose is the primary energy source for homeostasis. Glucose transport across the plasma membrane *via* a glucose transporter (GLUT) is a rate-limiting step in glucose metabolism.[17] AMP-activated protein kinase (AMPK), a serine threonine kinase, has been shown to regulate glucose uptake by facilitating the translocation of the GLUT to the membrane or by activation of transporter activity at the plasma membrane.[18,19] The fetal brain has been reported to rely on anaerobic glycolysis to meet its energy demands.[20] Thus, GLUT is considered essential in the early organogenesis period. GLUT1, a major subtype of GLUT in fetal tissue, has been shown to mediate organogenesis in rat embryos.[21] In addition, clinical data regarding human GLUT1 deficiency syndrome suggest that GLUT1 is necessary for human brain development.[22]

In the present study, we hypothesized a possible link between TBT toxicity and glucose metabolism. We found that

[a] *Division of Pharmacology, National Institute of Health Sciences, 1-18-1, Kamiyoga, Setagaya-ku 158-8501, Japan. E-mail: kanda@nihs.go.jp; Fax: +81-3-3700-9704; Tel: +81-3-3700-9704*

[b] *Department of Xenobiotic Metabolism and Molecular Toxicology, Graduate School of Biomedical and Health Sciences, Hiroshima University, Japan*

† Electronic supplementary information (ESI) available. See DOI: 10.1039/c3mt20268b

exposure to TBT reduced the amounts of glucose-6-phosphate and fructose-6-phosphate *via* a decrease in surface-bound GLUT1 in the human pluripotent embryonic carcinoma cell line NT2/D1. In addition, treatment with the potent AMPK activator, 5-aminoimidazole-4-carboxyamide ribonucleoside (AICAR), restored the inhibitory effect of TBT on both cell surface-bound GLUT1 levels and glucose uptake. We report here that the glycolytic pathway is a molecular target of nanomolar levels of TBT in human embryonic carcinoma cells.

Methods

Cell culture

NT2/D1 cells were obtained from the American Type Culture Collection. The cells were cultured in Dulbecco's modified Eagle's medium (DMEM; Sigma-Aldrich, St. Louis, MO, USA) supplemented with 10% fetal bovine serum (FBS; Biological Industries, Ashrat, Israel) and 0.05 mg mL^{-1} penicillin–streptomycin mixture (Life Technologies, Carlsbad, CA, USA) at 37 °C and 5% CO_2. For neural differentiation, all-trans retinoic acid (RA; Sigma-Aldrich) was added to the medium twice a week at a final concentration of 10 μM.

Cell proliferation assay

Cell viability was measured using the CellTiter 96 AQueous One Solution Cell Proliferation Assay (Promega, Madison, WI, USA), according to the manufacturer's instructions. Briefly, NT2/D1 cells were seeded into 96-well plates and exposed to different concentrations of TBT. After exposure to TBT, One Solution Reagent was added to each well, and the plate was incubated at 37 °C for another 2 h. Absorbance was measured at 490 nm using an iMark microplate reader (Bio-Rad, Hercules, CA, USA).

Glucose uptake assay

A glucose uptake assay was performed using a fluorescent glucose derivative, 2-[*N*-(7-nitrobenz-2-oxa-1,3-diazol-4-yl)amino]-2-deoxy-D-glucose (2-NBDG; Peptide Institute Inc., Osaka, Japan) by the previously reported procedure with slight modifications.[23] Briefly, NT2/D1 cells exposed to TBT were incubated with 2-NBDG (100 μM) for 2 h at 37 °C. The 2-NBDG uptake reaction was stopped by draining the incubation medium and washing the cells twice with ice-cold PBS. The incorporated 2-NBDG was measured using a Wallac1420ARVO fluoroscan (Perkin-Elmer, Waltham, MA, USA) with excitation at 488 nm and emission at 515 nm. The fluorescence intensities were normalized to the total protein content.

Hexokinase activity assay

Hexokinase activity was determined using a commercial Hexokinase Colorimetric Assay Kit (Biovision, Mountain View, CA, USA), according to the manufacturer's instructions.

AMPK activity assay

AMPK activity was determined using a commercial CycLex AMP Kinase Assay Kit (MBL International, Woburn, MA, USA), according to the manufacturer's instructions.

Determination of glucose-6-phosphate and fructose-6-phosphate

Intracellular metabolites were extracted and used for subsequent capillary electrophoresis time-of-flight mass spectrometry (CE-TOFMS) analysis, as described previously.[24] Glucose-6-phosphate and fructose-6-phosphate were determined using an Agilent CE capillary electrophoresis system (Agilent Technologies, Waldbronn, Germany) equipped with an Agilent G3250AA LC/MSD TOF system (Agilent Technologies, Palo Alto, CA), an Agilent 1100 series isocratic HPLC pump, a G1603A Agilent CE-MS adapter kit, and a G1607A Agilent CE-electrospray ionization 53-MS sprayer kit. For system control and data acquisition, G2201AA Agilent ChemStation software was used for CE, and Agilent TOF (Analyst QS) software was used for TOFMS.

Western blotting

Western blotting was performed as previously reported.[25] Briefly, the cells were lysed using Cell Lysis Buffer (Cell Signaling Technology, Danvers, MA, USA), and proteins were then separated by sodium dodecyl sulfate (SDS)-polyacrylamide gel electrophoresis and electrophoretically transferred to Immobilon-P membranes (Millipore, Billerica, MA, USA). The membranes were probed using primary antibodies (anti-GLUT1 polyclonal antibodies [1 : 200; Santa Cruz Biotechnology, Santa Cruz, CA, USA], anti-c-Myc polyclonal antibodies [1 : 1000; Sigma-Aldrich], anti-Flag monoclonal antibodies [1 : 1000; Sigma-Aldrich], and anti-β-actin monoclonal antibodies [1 : 1000; Sigma-Aldrich]). The membranes were then incubated with secondary antibodies against rabbit or mouse IgG conjugated with horseradish peroxidase (Cell Signaling Technology). The bands were visualized using an ECL Western Blotting Analysis System (GE Healthcare, Buckinghamshire, UK), and images were acquired using a LAS-3000 Imager (Fujifilm UK Ltd., Systems, Bedford, UK). The density of each band was quantified with ImageJ software (NIH, Bethesda, MD, USA).

Cell surface biotinylation

NT2/D1 cell surface proteins were biotinylated using a Cell Surface Protein Isolation Kit, according to the manufacturer's instructions (Pierce, Rockford, IL, USA). Briefly, cells were incubated with ice-cold phosphate-buffered saline (PBS; pH 7.4) containing Sulfo-NHS-SS-Biotin, with gentle rocking for 30 min at 4 °C. The biotinylated proteins were precipitated with streptavidin beads and eluted from the beads with SDS sample buffer. The proteins were analyzed by western blotting with anti-GLUT1 antibodies.

Immunohistochemistry

Cells, cultured on glass coverslips, were fixed in 4% paraformaldehyde in PBS (pH 7.4) for 15 min at room temperature. The fixed cells were incubated with anti-GLUT1 polyclonal antibodies (1 : 100; Santa Cruz) for 1 h at room temperature. Finally, they were incubated with Alexa488-conjugated secondary antibodies (1 : 200; Life Technologies) for 1 h at room temperature. The cells were enclosed in SlowFade (Life Technologies) and examined under a BIOREVO BZ-9000 fluorescent microscope (Keyence, Osaka, Japan).

Transfection

Cells were transiently transfected with Flag-tagged GLUT1 in pEF6 (a kind gift from Dr Rathmell) and c-Myc-tagged constitutively active-AMPK-α1 (T172D) or c-Myc-tagged dominant-negative-AMPK-α1 (K45R) in pcDNA3 (a kind gift from Dr Carling) using the FuGene HD Transfection Reagent (Promega), according to the manufacturer's protocol. After 48 h incubation, the transfectants were cultured with 12.5 μg mL^{-1} blasticidin or 0.5 mg mL^{-1} G418.

Real-time PCR

After total RNA was isolated from NT2/D1 cells using TRIzol (Life Technologies), quantitative real-time reverse transcription (RT)-PCR with a QuantiTect SYBR Green RT-PCR Kit (QIAGEN, Valencia, CA, USA) was performed using an ABI PRISM 7900HT sequence detection system (Applied Biosystems, Foster City, CA, USA), as previously reported.[26] The relative changes in the amounts of transcripts in each sample were normalized using ribosomal protein L13 (RPL13) mRNA levels. The sequences of the primers used for real-time PCR analysis are as follows: GLUT1 (forward, 5′-CCAGCTGCCATTGCCGTT-3′; reverse, 5′-GACGTAGGGACCACACAGTTGC-3′), GLUT2 (forward, 5′-CACACAAGACCTGGAATTGACA-3′; reverse, 5′-CGGTCATCCAGTGGAACAC-3′), GLUT3 (forward, 5′-CAATGCTCCTGAGAAGATCATAA-3′; reverse, 5′-AAAGCGGTTGACGAAGAGT-3′), GLUT4 (forward, 5′-CTGGGCCTCACAGTGCTAC-3′; reverse, 5′-GTCAGGCGCTTCAGACTCTT-3′), nestin (forward, 5′-GGCAGCGTTGGAACAGAGGT-3′; reverse, 5′-CATCTTGAGGTGCGCCAGCT-3′), NeuroD (forward, 5′-GGAAACGAACCCACTGTGCT-3′; reverse, 5′-GCCACACCAAATTCGTGGTG-3′), Math1 (forward, 5′-GTCCGAGCTGCTACAAACG-3′; reverse, 5′-GTGGTGGTGGTCGCTTTT-3′), MAP2 (forward, 5′-CCAATGGATTCCCATACAGG-3′; reverse, 5′-CTGCTACAGCCTCAGCAGTG-3′), RPL13 (forward, 5′-CATCGTGGCTAAACAGGTACTG-3′; reverse, 5′-GCACGACCTTGAGGGCAGCC-3′).

Materials

TBT was obtained from Tokyo Chemical Industry (Tokyo, Japan). Tin acetate (TA), AICAR, and rosiglitazone were obtained from Sigma-Aldrich. All other reagents were of analytical grade and obtained from commercial sources.

Statistical analysis

All data were presented as mean ± S.D. ANOVA followed by a *post hoc* Tukey test was used to analyze data in Fig. 1–4. Unpaired Student's *t* test was used to analyze data in Fig. 5. A *p* value of less than 0.05 was considered significant.

Results

To examine the effect of TBT on the proliferation of human NT2/D1 embryonic carcinoma cells, we exposed the cells to different concentrations of TBT for 24 h and measured cell viability by MTT assay. Treatment with TBT reduced cell viability in a dose-dependent manner (Fig. 1A; 0.03–0.3 μM). We observed that almost all cells were detached from the culture dish at TBT concentrations of 300 nM and above. In contrast, the less toxic TA had little effect at any concentration (Fig. 1A–e). We performed time-course experiments with 100 nM TBT, and determined the cell number. Exposure to

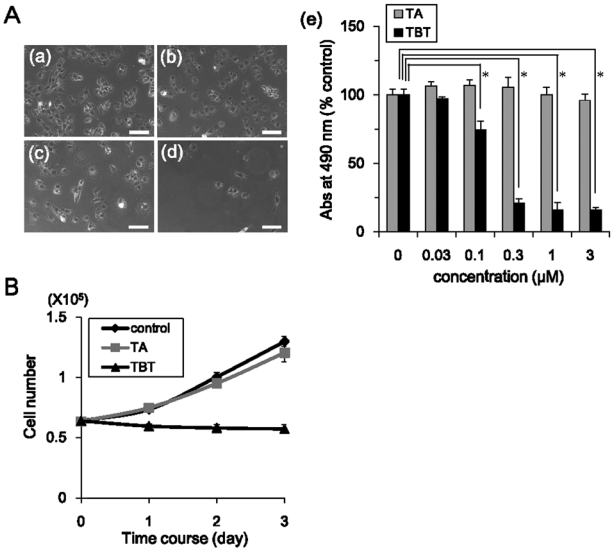

Fig. 1 Effect of TBT exposure on cell proliferation in NT2/D1 cells. (A) NT2/D1 cells were seeded into 96-well plates and exposed to TBT at different concentrations for 24 h. (a–d) Phase-contrast photomicrographs of NT2/D1 cells exposed to TBT at 0, 0.03, 0.1, or 0.3 μM (Bar = 100 μm). (e) Cell viability in the presence of TBT or TA was examined using the CellTiter 96 AQueous One Solution Cell Proliferation Assay. (B) NT2/D1 cells (6×10^5 cells) were seeded into 100 mm dishes and exposed to 100 nM TBT. After 24, 48, and 72 h, cell count was determined using a hemocytometer. *$P < 0.05$.

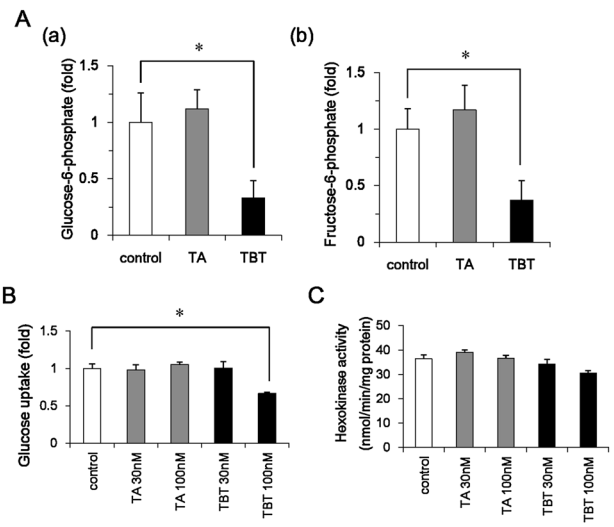

Fig. 2 Effect of TBT exposure on glycolytic systems in NT2/D1 cells. (A) After 24 h exposure to 100 nM TBT or TA, glucose 6-phosphate (a) and fructose 6-phosphate (b) levels were determined using CE-TOFMS. (B) After exposure to TBT or TA (30, 100 nM) for 24 h, glucose uptake assay was performed using a fluorescent glucose analog 2-NBDG. The fluorescence intensities of incorporated 2-NBDG were normalized to total cellular protein content. (C) After exposure to TBT or TA (30, 100 nM) for 24 h, hexokinase activity was measured using a commercial assay kit. *$P < 0.05$.

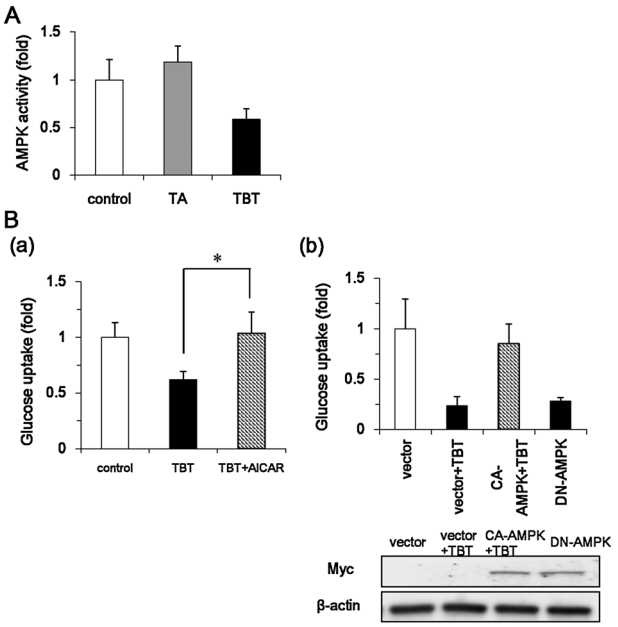

Fig. 3 Effect of AMPK on glucose uptake in NT2/D1 cells. (A) NT2/D1 cells were exposed to TBT or TA at 100 nM for 24 h. AICAR (0.5 mM) treatment was performed for 3 h. AMPK activity in the lysed cells was determined using a commercial assay kit. (B) NT2/D1 cells were exposed to TBT in the presence of 0.5 mM AICAR. (C) After overexpression of constitutively active (CA) mutants of AMPK, NT2/D1 cells were exposed to 100 nM TBT for 24 h, and glucose uptake assay was performed. After overexpression of dominant-negative (DN) mutants of AMPK, basal glucose uptake was tested. A glucose uptake assay was performed using the fluorescent glucose analog 2-NBDG. The fluorescence intensities of incorporated 2-NBDG were normalized to total cellular protein content. $^*P < 0.05$.

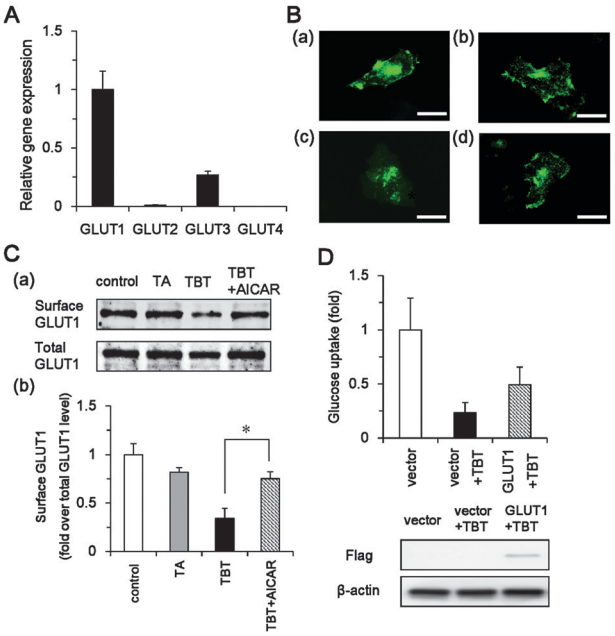

Fig. 4 Effect of TBT exposure on GLUT1 localization in NT2/D1 cells. (A) Expression of GLUT family by real-time PCR in NT2/D1 cells. Relative changes were determined by normalizing to RPL13. (B) After exposure to 100 nM TBT for 24 h, NT2/D1 cells were immunostained with anti-GLUT1 polyclonal antibodies. (a) Control, (b) 100 nM TA, (c) 100 nM TBT, and (d) 100 nM TBT + 0.5 mM AICAR. (Bar = 25 μm). (C) (a) NT2/D1 cell surface proteins were biotinylated using Sulfo-NHS-SS-Biotin, and then lysed. After precipitation with streptavidin beads, biotinylated proteins were analyzed by western blotting using anti-GLUT1 antibodies. Total GLUT1 protein was detected in cell lysate. (b) The relative density of bands was quantified with ImageJ software. Cell surface GLUT1 levels were normalized to total GLUT1 levels. (D) After overexpression of GLUT1, NT2/D1 cells were exposed to 100 nM TBT for 24 h, and glucose uptake assay was performed using the fluorescent glucose analog 2-NBDG. The fluorescence intensities of incorporated 2-NBDG were normalized to total cellular protein content. $^*P < 0.05$.

TBT suppressed the growth curve, but the total cell number did not alter throughout the time-course experiment (Fig. 1B). These data suggest that exposure to 100 nM TBT induced growth arrest in the cells without causing cell death.

Glucose provides metabolic energy for cell growth and it is incorporated by glucose transporters.[17] To examine the mechanism by which TBT induces growth arrest at low concentrations, we determined the glucose-6-phosphate, a major metabolite in glycolysis. We found that exposure to 100 nM TBT reduced the amount of glucose-6-phosphate (Fig. 2A). Fructose-6-phosphate, which is produced by isomerization of glucose 6-phosphate, also reduced by TBT. To check whether the decrease in glucose-6-phosphate is induced by inhibition of glucose transport, we examined the activity of glucose uptake by using 2-NBDG, a fluorescently labeled 2-deoxyglucose. Similar to the cell growth, glucose uptake was significantly inhibited by 100 nM TBT, not by 30 nM TBT (Fig. 2B). TA had little effect on glucose uptake. To examine whether the inhibition is regulated by transcription, we tested the effect of short-term exposure. Exposure to TBT for 1 h suppressed glucose uptake (Fig. S1, ESI†), suggesting that gene expression is not involved in the effect of TBT. Since TBT has been shown to activate transcriptional activity of peroxisome proliferator-activated receptor γ (PPARγ),[27,28] we tested the effect of the PPARγ agonist rosiglitazone on the glucose uptake. Treatment with rosiglitazone increased glucose uptake (Fig. S2, ESI†), suggesting that PPARγ is not involved in TBT-induced inhibition of glucose uptake. Furthermore, we examined the activity of hexokinase, which catalyzes the phosphorylation of glucose into glucose-6-phosphate. As shown in Fig. 2C, hexokinase activity was not significantly altered by TBT. Exposure to TA also produced similar results. These data suggest that TBT exposure decreases the amount of glycolytic metabolites *via* inhibition of glucose transport.

AMP-activated protein kinase (AMPK) is known to regulate the translocation of a glucose transporter (GLUT) to the plasma membrane.[29] We examined whether AMPK is involved in the inhibition of glycolytic systems by TBT exposure. Exposure to 100 nM TBT reduced AMPK activity (Fig. 3A). In contrast, TA had little effect on AMPK. In addition, treatment with AICAR (a potent AMPK activator) recovered the inhibitory effect of TBT on glucose uptake (Fig. 3B). To confirm the effect of AICAR, we examined the effect of constitutively active (CA) mutants of AMPK. Similar to the treatment with AICAR, overexpression of CA-AMPK recovered the inhibitory effect of TBT on glucose uptake. Overexpression of dominant-negative mutants of AMPK reduced the basal level of glucose uptake, suggesting that

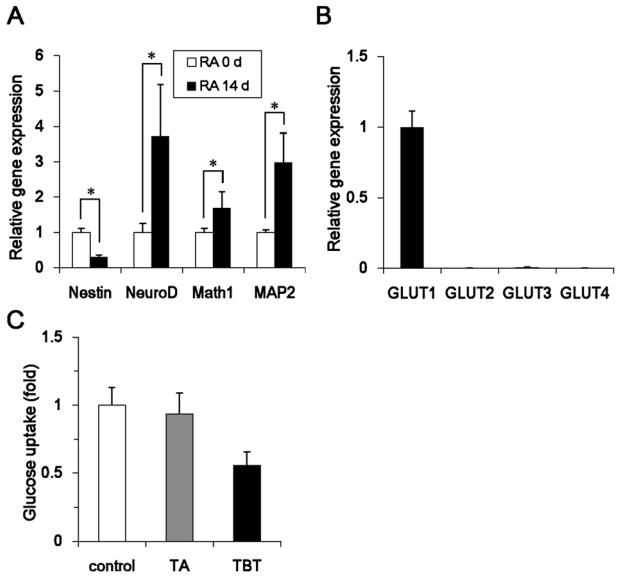

Fig. 5 Effect of neuronal induction on glucose uptake under TBT exposure in NT2/D1 cells. (A) To induce neuronal differentiation, NT2/D1 cells were treated with 10 μM RA for 14 days. The relative expression of neuronal markers (NeuroD, Math1, and MAP2) and a marker of undifferentiation (nestin) were measured by real-time-PCR. The relative changes were normalized to RPL13. (B) Expressions of members of the GLUT family were measured by real-time PCR in differentiated NT2/D1 cells. Relative changes were determined by normalizing to RPL13. (C) After exposure to 100 nM TBT for 24 h, glucose uptake was measured in differentiated cells. The fluorescence intensities of intracellularly incorporated 2-NBDG were measured and normalized to the total cellular protein levels. $^{*}P < 0.05$.

glucose uptake is AMPK-dependent in NT2/D1 cells. Taken together, these data suggest that TBT exposure suppresses glucose uptake through the inhibition of AMPK activity.

We next examined the mechanism by which AMPK regulates glucose uptake in NT2/D1 cells. Real-time PCR analysis showed that GLUT1 was a major subtype in NT2/D1 cells (Fig. 4A). Since TBT exposure did not affect gene expression of GLUT1 (data not shown), we examined GLUT1 localization by immunohistochemistry. Expression of GLUT1 was observed at the plasma membrane and in the intracellular segment (Fig. 4B). Exposure with TBT reduced the cell surface expression of GLUT1. Treatment with AICAR recovered the inhibitory effect of TBT. To confirm these observations using microscopy, we labeled cell surface-bound GLUT1 by biotinylation of cell surface proteins (Fig. 4C). Using this approach, we determined that TBT exposure reduced the amount of cell surface-bound GLUT1. AICAR reversed this inhibitory effect of TBT. Furthermore, overexpression of GLUT1 partially recovered the TBT-induced inhibition of glucose uptake (Fig. 4D). These data suggest that TBT inhibits glucose uptake mediated by cell surface translocation of GLUT1, a process dependent on AMPK.

To examine whether the effect of TBT was selective for embryonic cells, we used NT2/D1 cells differentiated by retinoic acid.[30] Real-time PCR analysis revealed that RA-treated NT2/D1 cells showed upregulated expression of markers of differentiation (NeuroD, Math1, MAP2) and downregulated expression of a marker of undifferentiation (nestin), confirming the induction of differentiation (Fig. 5A). Real-time PCR confirmed that GLUT1 is a major subtype in the differentiated NT2/D1 cells (Fig. 5B). Furthermore, exposure to 100 nM TBT also reduced glucose uptake in differentiated NT2/D1 cells. In contrast, TA had little effect (Fig. 5C). These data suggest that TBT suppresses glucose uptake in both undifferentiated and differentiated cells.

Discussion

In the present study, we showed that the glycolytic pathway is a novel target of TBT toxicity in human embryonic carcinoma cells. We showed that TBT suppresses AMPK-dependent glucose uptake, and thereby, the amount of glucose-6-phosphate. The inhibitory effects of TBT on glycolytic systems would lead to growth arrest in the cells. Fig. 6 shows a proposed model of TBT-induced toxicity, based on the data observed in our study.

Our studies showed that treatment with 1 μM TBT resulted in the death of human embryonic carcinoma cells (Fig. 1). Consistent with these observations, previous studies have shown that micromolar levels of TBT induce apoptosis in various cells such as human amnion cells,[31] hepatocytes,[32] and neutrophils.[33] In contrast, exposure to 100 nM TBT resulted in neither growth arrest nor cell death. Therefore, we focused on intracellular metabolites as potential mediators of TBT-induced growth arrest. We found that exposure to nanomolar levels of TBT affects the intracellular metabolic balance and decreases the amount of glucose metabolites (Fig. 2). A previous report showed that the organotin compounds such as TBT might be present in human blood at nanomolar levels.[16] Glucose metabolism analysis revealed novel toxic mechanisms

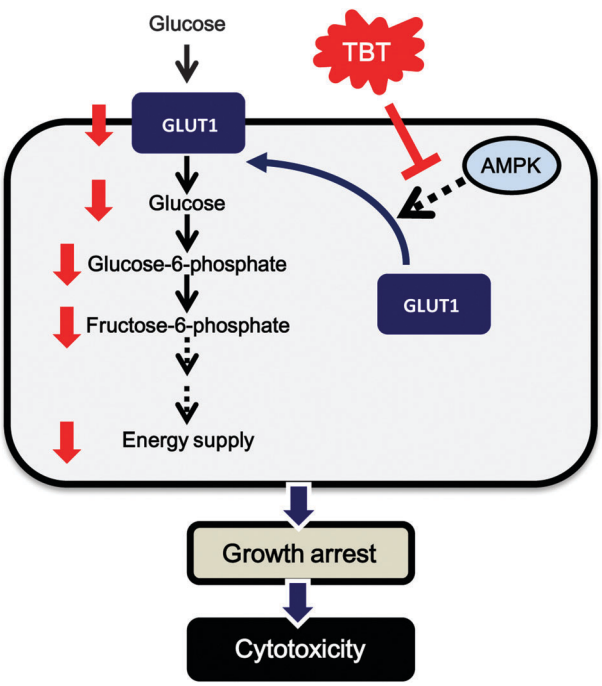

Fig. 6 Proposed model of TBT toxicity in human embryonic carcinoma cells.

for the toxicity of nanomolar levels of TBT. Thus, the glycolytic pathway might account for the unknown toxic mechanism induced by heavy metal exposure.

Our data suggest that the target molecule of TBT toxicity is GLUT1, a major subtype of GLUT in NT2/D1 cells (Fig. 4). Since the expression of GLUT1 is observed in a broad range of cell types, the toxicity of TBT may also be observed in other cells. For example, we showed that TBT reduces glucose uptake in differentiated NT2/D1 cells, which express GLUT1 (Fig. 5). Thus, it is possible that TBT induces toxicity in mature neurons *via* inhibition of GLUT function.

We showed that TBT decreases AMPK activity, one of the GLUT regulators, in NT2/D1 cells (Fig. 3). In addition, overexpression of AMPK or the AMPK activator restored the glucose uptake, confirming that AMPK is a possible target of TBT. In contrast, 500 nM TBT has been shown to increase AMPK phosphorylation in rat cortical neurons.[34] This discrepancy might be due to the concentration of TBT or different types of cells.

Several studies suggest that TBT directly interacts with target enzymes. TBT at a concentration of 10–100 nM has been shown to act as an agonist of PPARγ and the retinoid X receptor (RXR) because of its higher binding affinity compared to intrinsic ligands. Other studies reported that micromolar concentrations of TBT inhibit F1F0 ATP synthase and 11β-hydroxysteroid dehydrogenase by direct interaction.[35,36] Therefore, TBT can bind to multiple targets with broad specificity. It is possible that TBT also interacts with AMPK. On the other hand, calmodulin-dependent protein kinase II (CaMK II) and serine–threonine liver kinase B1 (LKB1) have been shown to phosphorylate AMPK and cause subsequent activation of glucose transport.[29] Furthermore, there may be an additional signaling molecule between TBT and AMPK. It remains to be elucidated how TBT regulates AMPK in embryonic carcinoma cells.

Nanomolar levels of TBT may interact with several targets in other types of cells, such as PPARγ, RXR, and α-amino-3-hydroxy-5-methylisoxazole-4-propionic acid (AMPA) receptors 2 (GluR2). Since rosiglitazone, a PPARγ agonist, increased glucose transport in NT2/D1 cells (Fig. S2, ESI†), it is unlikely that TBT inhibits glucose transport *via* PPARγ in the cells. RXR transgenic mice have been shown to exhibit an increase in GLUT1 expression in the skeletal muscles.[37] Since the expression level of GLUT1 was not changed by TBT exposure in NT2/D1 cells and the inhibitory effect of glucose uptake was observed after a 1 h treatment with TBT, it is likely that RXR is not involved in TBT-mediated alteration of glucose transport. Moreover, exposure to nanomolar levels of TBT has been reported to decrease the mRNA expression of GluR2 in cultured rat cortical neurons.[38] Although NT2/D1 cells do not express GluR2, it is possible that GluR2 may be a target in the differentiated NT2/D1 cells. Further studies are required to examine these targets other than the glycolytic pathway.

Conclusions

We found that exposure to nanomolar levels of TBT mainly targets the glycolytic systems in human embryonic carcinoma cells. Thus, glycolytic systems may be a good target for previously unknown mechanisms of toxicity induced by metal exposure at nanomolar levels.

Conflict of interest

The authors declare that there are no conflicts of interest.

List of abbreviations

AMPK	AMP-activated protein kinase
GLUT	glucose transporter
RA	all-trans retinoic acid
PPARγ	peroxisome proliferator-activated receptor γ
TA	tin acetate
TBT	tributyltin

Acknowledgements

We would like to thank Dr Rathmell and Dr Carling for providing the materials. This study was supported in part by a Health and Labour Sciences Research Grant from the Ministry of Health, Labour and Welfare, Japan (Y. Ka.), a grant from the Program for Promotion of Fundamental Studies in Health Sciences of the National Institute of Biomedical Innovation (NIBIO) (No. 09-02 to Y. Ka.), Grants-in-Aid for Scientific Research (No. 23590322 to Y. Ka. and No. 23310047 to Y. Ko.) from the Japan Society for the Promotion of Science, and a grant from the Smoking Research Foundation (Y. Ka.).

References

1 H. L. Needleman, C. Gunnoe, A. Leviton, R. Reed, H. Peresie, C. Maher and P. Barrett, Deficits in psychologic and classroom performance of children with elevated dentine lead levels, *N. Engl. J. Med.*, 1979, **300**, 689–695.
2 G. Winneke, Developmental aspects of environmental neurotoxicology: lessons from lead and polychlorinated biphenyls, *J. Neurol. Sci.*, 2011, **308**, 9–15.
3 L. G. Costa, M. Aschne, A. Vitalone, T. Syversen and O. P. Soldin, Developmental neuropathology of environmental agents, *Annu. Rev. Pharmacol. Toxicol.*, 2004, **44**, 87–110.
4 J. Dobbing, *Vulnerable periods in developing brain*, in *Appl. Neurochem.*, ed. A. N. Davison and J. Dobbing, Davis, Philadelphia, 1968, pp. 287–316.
5 P. M. Rodier, Developing brain as a target of toxicity, *Environ. Health Perspect.*, 1995, **103**(suppl 6), 73–76.
6 D. Rice and S. Barone Jr, Critical periods of vulnerability for the developing nervous system: evidence from humans and animal models, *Environ. Health Perspect.*, 2000, **108**(suppl 3), 511–533.
7 H. Asakawa, M. Tsunoda, T. Kaido, M. Hosokawa, C. Sugaya, Y. Inoue, Y. Kudo, T. Satoh, H. Katagiri, H. Akita, M. Saji, M. Wakasa, T. Negishi, T. Tashiro and Y. Aizawa, Enhanced

inhibitory effects of TBT chloride on the development of F1 rats, *Arch. Environ. Contam. Toxicol.*, 2010, **58**, 1065–1073.
8 S. Gómez-Ruiz, G. N. Kaluderović, S. Prashar, E. Hey-Hawkins, A. Erić, Z. Zizak and Z. D. Juranić, Study of the cytotoxic activity of di and triphenyltin(IV) carboxylate complexes, *J. Inorg. Biochem.*, 2008, **102**, 2087–2096.
9 L. Rocamora-Reverte, E. Carrasco-García, J. Ceballos-Torres, S. Prashar, G. N. Kaluđerović, J. A. Ferragut and S. Gómez-Ruiz, Study of the anticancer properties of tin(IV) carboxylate complexes on a panel of human tumor cell lines, *ChemMedChem*, 2012, **7**, 301–310.
10 A. González, E. Gómez, A. Cortés-Lozada, S. Hernández, T. Ramírez-Apan and A. Nieto-Camacho, Heptacoordinate tin(IV) compounds derived from pyridine Schiff bases: synthesis, characterization, *in vitro* cytotoxicity, anti-inflammatory and antioxidant activity, *Chem. Pharm. Bull.*, 2009, **57**, 5–15.
11 Y. Kotake, Molecular mechanisms of environmental organotin toxicity in mammals, *Biol. Pharm. Bull.*, 2012, **35**, 1876–1880.
12 T. Noda, S. Morita, T. Yamano, M. Shimizu, T. Nakamura, M. Saitoh and A. Yamada, Teratogenicity study of tri-*n*-butyltin acetate in rats by oral administration, *Toxicol. Lett.*, 1991, **55**, 109–115.
13 A. T. Gardlund, T. Archer, K. Danielsen, B. Danielsson, A. Frederiksson, N. G. Lindquist, H. Lindstrom and J. Luthman, Effects of prenatal exposure to tributyltin and trihexyltin on behavior in rats, *Neurotoxicol. Teratol.*, 1991, **13**, 99–105.
14 Q. Li, M. Osada, K. Takahashi, T. Matsutani and K. Mori, Accumulation and depuration of tributyltin oxide and its effect on the fertilization and embryonic development in the pacific oyster, *Crassostrea gigas*, *Bull. Environ. Contam. Toxicol.*, 1997, **58**, 489–496.
15 Y. Nakatsu, Y. Kotake, K. Komasaka, H. Hakozaki, R. Taguchi, T. Kume, A. Akaike and S. Ohta, Glutamate excitotoxicity is involved in cell death caused by tributyltin in cultured rat cortical neurons, *Toxicol. Sci.*, 2006, **89**, 235–242.
16 M. M. Whalen, B. G. Loganathan and K. Kannan, Immunotoxicity of environmentally relevant concentrations of butyltins on human natural killer cells *in vitro*, *Environ. Res. Lett.*, 1999, **81**, 108–116.
17 L. Pellerin, Food for thought: the importance of glucose and other energy substrates for sustaining brain function under varying levels of activity, *Diabetes Metab.*, 2010, **36**, S59–S63.
18 K. Barnes, J. C. Ingram, O. H. Porras, L. F. Barros, E. R. Hudson, L. G. Fryer, F. Foufelle, D. Carling, D. G. Hardie and S. A. Baldwin, Activation of GLUT1 by metabolic and osmotic stress: potential involvement of AMP-activated protein kinase (AMPK), *J. Cell Sci.*, 2002, **115**, 2433–2442.
19 M. Jing, V. K. Cheruvu and F. Ismail-Beigi, Stimulation of glucose transport in response to activation of distinct AMPK signaling pathways, *Am. J. Physiol.: Cell Physiol.*, 2008, **295**, C1071–C1082.
20 B. Kunievsky, J. Pretsky and E. Yavin, Transient rise of glucose uptake in the fetal rat brain after brief episodes of intrauterine ischemia, *Dev. Neurosci.*, 1994, **16**, 313–320.
21 K. Matsumoto, S. Akazawa, M. Ishibashi, R. A. Trocino, H. Matsuo, H. Yamasaki, Y. Yamaguchi, S. Nagamatsu and S. Nagataki, Abundant expression of GLUT1 and GLUT3 in rat embryo during the early organogenesis period, *Biochem. Biophys. Res. Commun.*, 1995, **209**, 95–102.
22 P. J. Jensen, J. D. Gitlin and M. O. Carayannopoulos, GLUT1 deficiency links nutrient availability and apoptosis during embryonic development, *J. Biol. Chem.*, 2006, **281**, 13382–13387.
23 Y. Kanda and Y. Watanabe, Thrombin-induced glucose transport *via* Src-p38 MAPK pathway in vascular smooth muscle cells, *Br. J. Pharmacol.*, 2005, **146**, 60–67.
24 T. Soga, Y. Ueno, H. Naraoka, Y. Ohashi, M. Tomita and T. Nishioka, Simultaneous determination of anionic intermediates for *Bacillus subtilis* metabolic pathways by capillary electrophoresis electrospray ionization mass spectrometry, *Anal. Chem.*, 2002, **74**, 2233–2239.
25 Y. Kanda and Y. Watanabe, Adrenaline increases glucose transport *via* a Rap1-p38MAPK pathway in rat vascular smooth muscle cells, *Br. J. Pharmacol.*, 2007, **151**, 476–482.
26 N. Hiarta, Y. Sekinoa and Y. Kanda, Nicotine increases cancer stem cell population in MCF-7 cells, *Biochem. Biophys. Res. Commun.*, 2010, **403**, 138–143.
27 T. Kanayama, N. Kobayashi, S. Mamiya, T. Nakanishi and J. Nishikawa, Organotin compounds promote adipocyte differentiation as agonists of the peroxisome proliferator-activated receptor gamma/retinoid X receptor pathway, *Mol. Pharmacol.*, 2005, **67**, 766–774.
28 F. Grün, H. Watanabe, Z. Zamanian, L. Maeda, K. Arima, R. Cubacha, D. M. Gardiner, J. Kanno, T. Iguchi and B. Blumberg, Endocrine-disrupting organotin compounds are potent inducers of adipogenesis in vertebrates, *Mol. Endocrinol.*, 2006, **20**, 2141–2155.
29 D. G. Hardie, F. A. Ross and S. A. Hawley, AMPK: a nutrient and energy sensor that maintains energy homeostasis, *Nat. Rev. Mol. Cell Biol.*, 2012, **13**, 251–262.
30 S. J. Pleasure, C. Page and V. M. Lee, Pure, postmitotic, polarized human neurons derived from NTera 2 cells provide a system for expressing exogenous proteins in terminally differentiated neurons, *J. Neurosci.*, 1992, **12**, 1802–1815.
31 X. Zhu, M. Xing, J. Lou, X. Wang, W. Fu and L. Xu, Apoptotic related biochemical changes in human amnion cells induced by tributyltin, *Toxicology*, 2007, **230**, 45–52.
32 M. Grondin, M. Marion, F. Denizeau and D. A. Averill-Bate, Tributyltin induces apoptotic signaling in hepatocytes through pathways involving the endoplasmic reticulum and mitochondria, *Toxicol. Appl. Pharmacol.*, 2007, **222**, 57–68.
33 V. Lavastre and D. Girard, Tributyltin induces human neutrophil apoptosis and selective degradation of cytoskeletal proteins by caspases, *J. Toxicol. Environ. Health, Part A*, 2002, **65**, 1013–1024.

34 Y. Nakatsu, Y. Kotake, A. Hino and S. Ohta, Activation of AMP-activated protein kinase by tributyltin induces neuronal cell death, *Toxicol. Appl. Pharmacol.*, 2008, **230**, 358–363.
35 C. von Ballmoos, J. Brunner and P. Dimroth, The ion channel of F-ATP synthase is the target of toxic organotin compounds, *Proc. Natl. Acad. Sci. U. S. A.*, 2004, **101**, 11239–11244.
36 A. G. Atanasov, L. G. Nashev, S. Tam, M. E. Baker and A. Odermatt, Organotins disrupt the 11β-hydroxysteroid dehydrogenase type 2-dependent local inactivation of glucocorticoids, *Environ. Health Perspect.*, 2005, **113**, 1600–1606.
37 S. Sugita, Y. Kamei, F. Akaike, T. Suganami, S. Kanai, M. Hattori, Y. Manabe, N. Fujii, T. Takai-Igarashi, M. Tadaishi, J. Oka, H. Aburatani, T. Yamada, H. Katagiri, S. Kakehi, Y. Tamura, H. Kubo, K. N. S. Miura, O. Ezaki and Y. Ogawa, Increased systemic glucose tolerance with increased muscle glucose uptake in transgenic mice overexpressing RXRγ in skeletal muscle, *PLoS One*, **6**, e20467.
38 Y. Nakatsu, Y. Kotake Y, T. Takishit and S. Ohta, Long-term exposure to endogenous levels of tributyltin decreases GluR2 expression and increases neuronal vulnerability to glutamate, *Toxicol. Appl. Pharmacol.*, 2009, **240**, 292–298.

SCIENTIFIC REPORTS

OPEN

SUBJECT AREAS:
METABOLOMICS
ENVIRONMENTAL SCIENCES

Received
17 February 2014

Accepted
15 July 2014

Published
5 August 2014

Correspondence and requests for materials should be addressed to Y.Ka (kanda@nihs.go.jp)

NAD-dependent isocitrate dehydrogenase as a novel target of tributyltin in human embryonic carcinoma cells

Shigeru Yamada[1], Yaichiro Kotake[2], Yosuke Demizu[3], Masaaki Kurihara[3], Yuko Sekino[1] & Yasunari Kanda[1]

[1]Division of Pharmacology, National Institute of Health Sciences, Tokyo, Japan, [2]Graduate School of Biomedical and Health Sciences, Hiroshima University, Hiroshima, Japan, [3]Division of Organic Chemistry, National Institute of Health Sciences, Tokyo, Japan.

Tributyltin (TBT) is known to cause developmental defects as endocrine disruptive chemicals (EDCs). At nanomoler concentrations, TBT actions were mediated by genomic pathways via PPAR/RXR. However, non-genomic target of TBT has not been elucidated. To investigate non-genomic TBT targets, we performed comprehensive metabolomic analyses using human embryonic carcinoma NT2/D1 cells. We found that 100 nM TBT reduced the amounts of α-ketoglutarate, succinate and malate. We further found that TBT decreased the activity of NAD-dependent isocitrate dehydrogenase (NAD-IDH), which catalyzes the conversion of isocitrate to α-ketoglutarate in the TCA cycle. In addition, TBT inhibited cell growth and enhanced neuronal differentiation through NAD-IDH inhibition. Furthermore, studies using bacterially expressed human NAD-IDH and *in silico* simulations suggest that TBT inhibits NAD-IDH due to a possible interaction. These results suggest that NAD-IDH is a novel non-genomic target of TBT at nanomolar levels. Thus, a metabolomic approach may provide new insights into the mechanism of EDC action.

Endocrine disruptive compounds (EDCs) have been studied extensively in environmental biology[1]. A large number of EDCs are known to cause genomic action via nuclear receptor. For example, xenoestrogens such as bisphenol A, genistein and diethylstilbestrol can bind to the estrogen receptor (ER) in the cell nucleus, followed by the alteration of gene expression[2,3]. In addition, EDCs induce the activation of non-genomic signaling pathways. For example, xenoestrogens increase intracellular calcium levels, activating eNOS and signaling cascades such as PI3K/AKT and MAPK[4–7]. Thus, both genomic and non-genomic pathways are required to understand the mechanism of EDC action.

Organotin compounds, such as tributyltin (TBT) are typical environmental contaminants and well known to cause developmental defects as EDCs. For example, TBT can cause increased fetal mortality, decreased fetal birth weights, and behavioral abnormalities in rat offspring[8,9]. Although the use of TBT has already been restricted, butyltin compounds, including TBT, can still be found in human blood at concentrations between 50 and 400 nM[10]. Several studies revealed that TBT activates retinoid X receptor (RXR) and/or peroxisome proliferator-activated receptor γ (PPARγ). These genomic transcriptional activations result in developmental effects, such as the imposex in many marine species[11–13] and the enhancement of adipocyte differentiation in mammals[14,15]. These TBT actions involve a higher binding affinity compared to intrinsic ligands at nM concentrations. In addition to the genomic effects, non-genomic action of TBT has been also reported. For example, TBT has been reported to inhibit the steroid biosynthesis pathway, which is responsible for the production of estrogen and androgen[16–18]. Another report has shown that TBT inhibits mitochondrial F1F0 ATP synthase[19]. These data were obtained at μM concentrations. Thus, the mechanism of nM concentrations of TBT has not been elucidated at a non-genomic level. In a previous study, we reported that treatment with 100 nM TBT resulted in growth arrest by targeting the glycolytic systems of the human embryonic carcinoma cell line NT2/D1[20]. Therefore, we raised the possibility that nM concentrations of TBT may target other non-genomic pathways which are involved in energy metabolism.

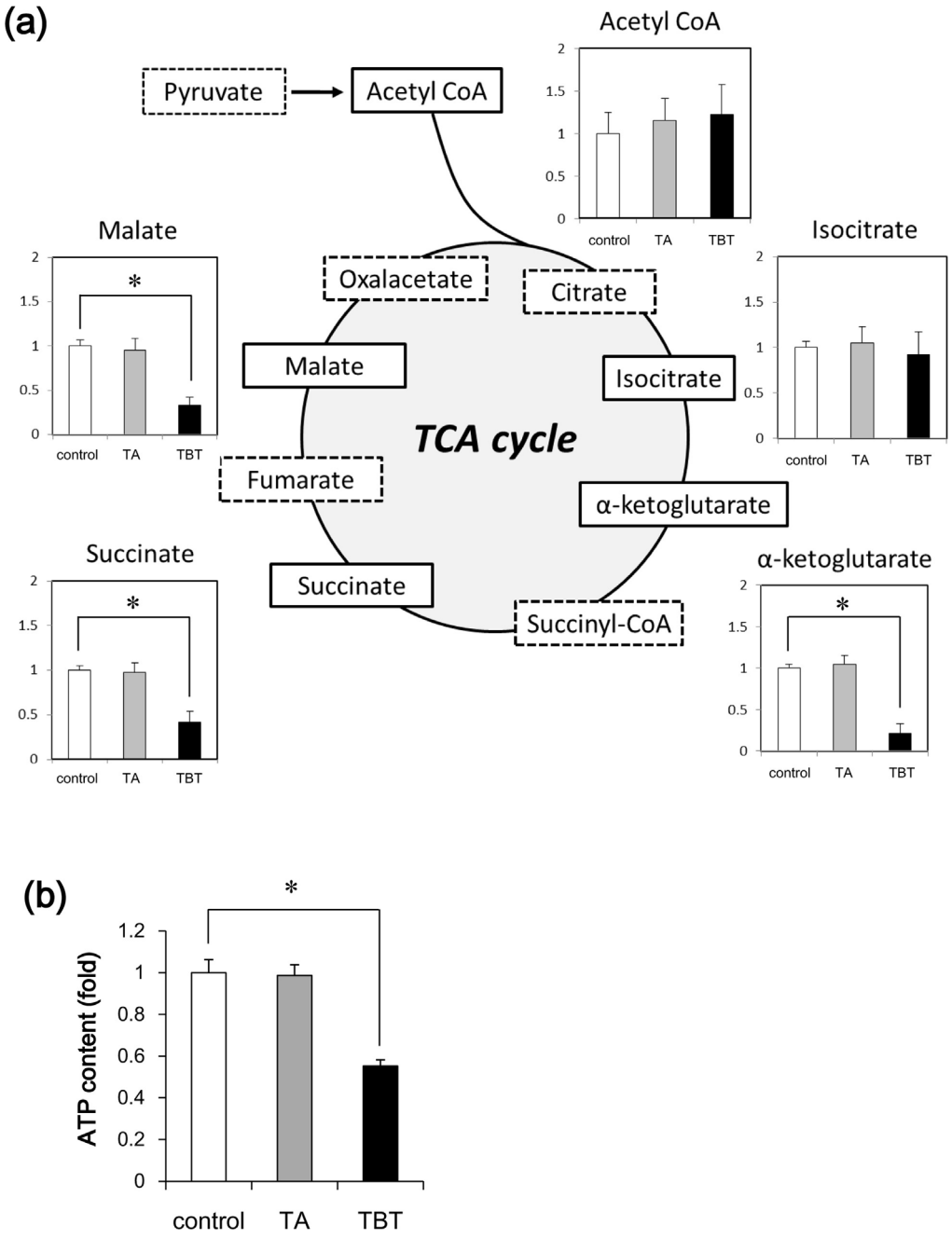

Figure 1 | **Metabolomic analysis of NT2/D1 cells exposed to TBT.** The cells were exposed to 100 nM TBT or TA for 24 h. (a) The levels of several metabolites, such as acetyl CoA, isocitrate, α-ketoglutarate, succinate and malate, were determined using CE-TOFMS. (b) The intracellular ATP content was determined in the lysed cells. * $P < 0.05$ compared with the corresponding control group.

In the present study, we investigated the molecular target of TBT at nM levels by comprehensive determination of the intracellular metabolites in NT2/D1 cells after TBT exposure. We found that exposure to 100 nM TBT reduced ATP production via NAD-dependent isocitrate dehydrogenase (NAD-IDH) in the cells. This NAD-IDH inhibition resulted in the reduction of the TCA cycle metabolites. In addition, TBT caused neural differentiation through an NAD-IDH-dependent mechanism. We report here that our metabolomic analysis revealed that NAD-IDH is a novel target of TBT in embryonic carcinoma cells.

Results

Metabolomic analysis of NT2/D1 cells exposed to TBT at nM levels. To investigate the non-genomic effects of a well-known endocrine disruptor TBT in human NT2/D1 embryonic carcinoma cells, we comprehensively determined intracellular metabolites using LC/MS. We found that exposure to 100 nM TBT reduced the amounts of TCA cycle components, such as α-ketoglutarate, succinate and malate (Figure 1a). The amounts of acetyl CoA and isocitrate were not changed. We also found that treatment with 100 nM TBT reduced the ATP content of the cells (Figure 1b). In contrast to TBT, exposure to the less toxic tin acetate (TA) did not affect the amount of each metabolite. These data suggest that TBT exposure decreases the amounts of TCA cycle metabolites, resulting in a reduction of ATP content.

NAD-IDH enzyme activity of NT2/D1 cells exposed to TBT at nM levels. Based on the results of the metabolomic analysis, we focused

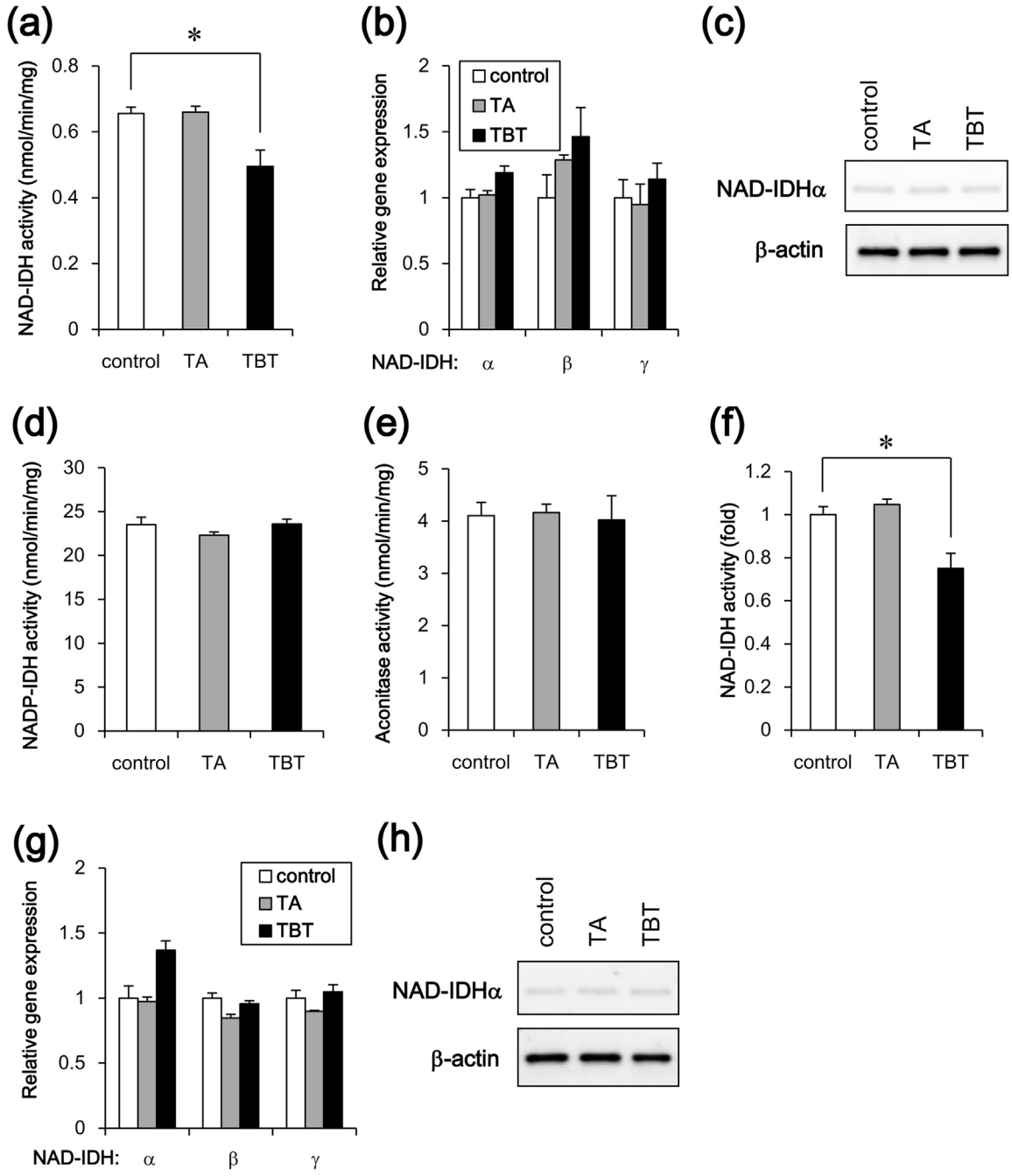

Figure 2 | Effect of TBT exposure on NAD-IDH enzyme activity in NT2/D1 cells. The cells were exposed to 100 nM TBT or TA for 24 h. (a) NAD-IDH activity was determined in the lysed cells. (b) The relative expressions of NAD-IDHα, β, and γ were measured using real-time PCR. The relative changes were normalized to the levels of RPL13. (c) The expression of NAD-IDHα protein was examined by western blot analysis using the anti-NAD-IDHα and anti-β-actin antibodies. Cropped blots were shown and the full-length blots were indicated in Supplementary Fig. 4. (d) NADP-IDH activity was determined in the lysed cells. (e) Aconitase activity was determined in the lysed cells. (f) To induce neuronal differentiation, the NT2/D1 cells were treated with 10 μM retinoic acid (RA) for 14 days. After exposure to 100 nM TBT for 24 h, NAD-IDH activity was determined in the lysed cells. (g) The relative expression levels of NAD-IDHα, β, and γ in the differentiated cells were measured using real-time PCR. The relative changes were normalized to the levels of RPL13. (h) The expression of NAD-IDHα protein was examined by western blot analysis using the anti-NAD-IDHα and anti-β-actin antibodies. Cropped blots were shown and the full-length blots were indicated in Supplementary Fig. 4. * $P < 0.05$ compared with the corresponding control group.

on isocitrate dehydrogenase, which catalyzes the conversion of isocitrate to α-ketoglutarate in the TCA cycle. Eukaryotes have different types of isocitrate dehydrogenases, such as NAD-dependent form (NAD-IDH; EC 1.1.1.41) and NADP-dependent form (NADP-IDH; EC 1.1.1.42)[21]. NAD-IDH is first rate-limiting enzyme in the TCA cycle and catalyzes an irreversible reaction, while NADP-IDH is involved in reversible reaction for biosynthesis via production of NADPH. As shown in Figure 2a, NAD-IDH activity was significantly reduced following TBT treatment. Since NAD-IDH is a heterotetramer composed of two α subunits (catalytic subunit), one β subunit and one γ subunit (regulatory subunit), we examined the expression of each subunit gene. Real-time PCR analysis showed

that the expression of the NAD-IDHα, β and γ genes was not significantly changed by TBT exposure (Figure 2b). The protein expression of catalytic α subunits was not also changed by TBT exposure (Figure 2c). TA exposure did not affect either the enzyme activity or the NAD-IDH expression. We next examined the effect of TBT on NADP-IDH. The activity of NADP-IDH was not affected by TBT exposure (Figure 2d). We further examined the activity of aconitase (EC 4.2.1.3.), which catalyzes the conversion of citrate to isocitrate in the TCA cycle. Aconitase activity was also not affected by TBT exposure (Figure 2e). Thus, these data suggest that the inhibitory effect of TBT is specific to NAD-IDH in the TCA cycle.

To investigate whether TBT cytotoxicity was caused by a genomic transcriptional regulation, we tested the effects of the protein synthesis inhibitor cycloheximide in NT2/D1 cells. Treatment with cycloheximide did not alter the inhibitory effects of TBT on NAD-IDH activity (Figure S1a) and intracellular ATP production (Figure S2a). Moreover, the PPARγ agonist rosiglitazone did not reduce NAD-IDH activity (Figure S1b) and ATP content (Figure S2b). These results suggest that transcriptional regulation is not involved in the inhibition of NAD-IDH activity by TBT.

To examine whether the effect of TBT was selective for embryonic cells, we used NT2/D1 cells that had differentiated in response to retinoic acid. We observed that TBT also inhibited NAD-IDH activity in the differentiated NT2/D1 cells (Figure 2f). Real-time PCR analysis showed that the expression of the NAD-IDHα, β, and γ genes was not significantly affected by TBT exposure (Figure 2g). The protein expression of catalytic α subunits was not also changed by TBT exposure (Figure 2h). TA exposure did not affect either the activity or the NAD-IDH expression. These data suggest that TBT reduces NAD-IDH enzyme activity regardless of the developmental stage of the embryonic carcinoma cells.

Neuronal differentiation of RA-treated NT2/D1 cells exposed to TBT at nM levels. It has been reported that ATP content decreases during the differentiation of human embryonic stem cells into neural stem cells (NSCs)[22]. Therefore, the reduction of ATP caused by TBT treatment might be involved in neuronal differentiation. Moreover, TBT has been reported to cause cell growth arrest in NT2/D1 cells[20]. Because cell growth is generally reduced during differentiation, we examined whether TBT affects the neuronal differentiation process in NT2/D1 cells. Real-time PCR analysis revealed that retinoic acid (RA)-treated NT2/D1 cells showed increased expression of the differentiation markers NeuroD and Math1, confirming that neural differentiation had occurred (Figure 3a). Furthermore, we observed that TBT exposure enhanced the expression levels of these neuronal differentiation markers. Treatment with rosiglitazone had little effect on their expression (Figure S3), suggesting that PPARγ is not involved in neuronal differentiation. Taken together, these data suggest that TBT promotes neuronal differentiation.

Effect of NAD-IDH knockdown on neuronal differentiation in RA-treated NT2/D1 cells. To further investigate whether the neuronal differentiation triggered by TBT exposure is through an NAD-IDH-dependent mechanism, we performed knockdown (KD) of NAD-IDHα, the catalytic subunit of NAD-IDH, using lentivirus-delivered shRNAs. Real-time PCR analysis showed that KD efficiency was approximately 40% (Figure 3b). Due to the partial KD of the NAD-IDHα gene, NAD-IDH activity decreased to a level (22%) comparable to its level following TBT inhibition (24%) (Figure 3c). Further reduction of NAD-IDH activity was not significantly observed after TBT exposure in the NAD-IDHα KD cells. Similar to the effect of TBT, NAD-IDHα KD also reduced the ATP content of the cells (Figure 3d), and caused cell growth inhibition (Figure 3e). Further inhibition of ATP content and cell growth was not significantly observed after TBT exposure in the NAD-IDHα KD cells, suggesting that the NAD-IDH is a possible target of TBT. In addition, we found that NAD-IDHα KD significantly upregulated the expression of the neuronal differentiation markers NeuroD and Math1 (Figure 3f). These data suggest that NAD-IDH mediates TBT-induced neuronal differentiation in embryonic NT2/D1 cells.

NAD-IDH enzyme activity in the brain of rats orally exposed to TBT at low doses. To examine whether the in vitro inhibitory effect of TBT on NAD-IDH is also observed in vivo, adult rats were orally exposed to TBT at doses of 5 and 50 mg/kg. NAD-IDH activity in the cerebral cortex was significantly reduced following exposure to both doses of TBT (Figure 4a). Real-time PCR analysis showed that the expression of the NAD-IDHα, β, and γ genes was not significantly affected by TBT (Figure 4b). The protein expression of catalytic α subunits was not also affected by TBT (Figure 4c). NADP-IDH and aconitase activities were not affected by exposure to either dose of TBT (Figure 4d and e). These data suggest that TBT inhibits NAD-IDH activity both in vitro and in vivo.

Reduction of recombinant hNAD-IDH enzyme activity in E. coli lysate treated with TBT at nM levels. To investigate the mechanism by which TBT inhibits NAD-IDH activity, we examined whether TBT possibly interacts with NAD-IDH or not. Since NAD-IDHα subunit alone has been reported to show no detectable IDH activity, we used an Escherichia coli co-expression system of recombinant human (h) NAD-IDHα,β,γ subunits[23]. As shown in Figure 5a, we confirmed the expression of α subunit of hNAD-IDH protein in the extracts of E. coli transformants using western blot analysis. To check the activity of the recombinant hNAD-IDH, we used irreversible and allosteric NAD-IDH regulators. ADP has been reported to activate NAD-IDH allosterically by lowering the Km for the substrate isocitrate[24]. As expected, ADP increased the activity of hNAD-IDH in our assay system. Conversely, Zn^{2+} has been reported to inhibit several metabolic enzymes, including NAD-IDH, in hepatocytes[25]. We confirmed that Zn^{2+} reduces hNAD-IDH activity. Then, we examined whether TBT directly inhibits hNAD-IDH activity by adding TBT to the E. coli extracts containing hNAD-IDH. Treatment with 100 nM TBT for 1 h significantly reduced the hNAD-IDH activity (Figure 5b). Treatment with TA had little effect. Taken together, these data suggest that TBT inhibits hNAD-IDH activity through its possible interaction, but again we can not be sure that it is through direct binding with the data we have.

***In silico* docking simulation analysis.** To further consider this possible interaction between TBT and hNAD-IDH, we estimate TBT accessibility into hNAD-IDH (EC 1.1.1.41) α and hNADP-IDH (EC 1.1.1.42) homodimers by homology modeling and docking studies. We show the overlaid structure of the calculated hNAD-IDHα and hNADP-IDH (Figure 6a). The ligand binding pocket of hNAD-IDHα was larger than that of hNADP-IDH (Figure 6b). In our docking simulation, TBT was able to access the hNAD-IDHα ligand-binding pocket, whereas the hNADP-IDH pocket was not spacious enough to accommodate TBT (Figure 6c and d). Thus, these studies suggest that the selective inhibition of NAD-IDH by TBT may be due to differences in the pocket volumes between hNAD-IDHα and hNADP-IDH.

Discussion

In the present study, we demonstrate that NAD-IDH is a novel non-genomic target of TBT at nM levels both in vitro and in vivo. We showed that exposure to nM concentrations of TBT reduced the activity of NAD-IDH due to its possible interaction. We also found that TBT exposure caused both inhibition of cell growth and enhancement of neuronal differentiation through its inhibitory effect of NAD-IDH.

Our data suggest that NAD-IDH is a novel target molecule of TBT action. NAD-IDH is a NAD-dependent form of IDH found in NT2/D1 cells and the rat brain (Figure 2–4). Because NAD-IDH is ubi-

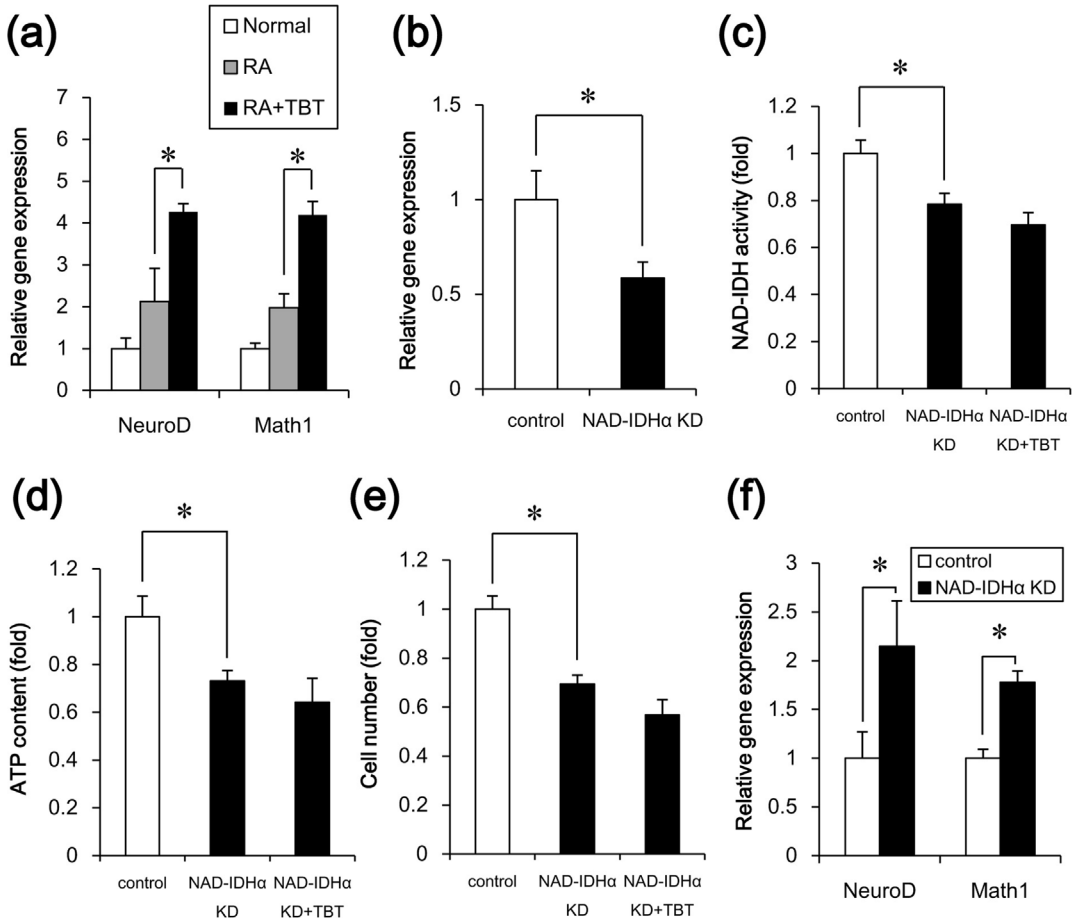

Figure 3 | Effect of TBT exposure or NAD-IDH knockdown on neuronal differentiation in RA-treated NT2/D1 cells. (a) After treatment with RA for 7 days, the cells were treated with RA in the presence of 100 nM TBT for an additional 7 days. The relative expression levels of the neuronal markers NeuroD and Math1 were measured using real-time PCR. The relative changes were determined following normalization to the levels of RPL13. (b–e) The cells were infected with lentiviruses containing a vector encoding a shRNA directed against NAD-IDHα or a scrambled sequence shRNA (control). The infected cells were subjected to selection with 0.5 μg/ml puromycin for 72 h and were then exposed to TBT at 100 nM for 24 h. (b) The relative expression of NAD-IDHα was measured using real-time PCR. The relative change in expression was normalized to the levels of RPL13. (c) NAD-IDH activity was determined in the lysed cells. (d) The intracellular ATP content was determined in the lysed cells. (e) Infected cells were seeded into 100 mm dishes and cultured for 24 h. Cell count was determined using a hemocytometer. (f) After treatment with RA for 7 days, followed by treatment with RA and the shRNA-containing lentiviruses for an additional 7 days, the relative expression levels of the neuronal markers NeuroD and Math1 were measured using real-time PCR. The relative changes were determined following normalization to the levels of RPL13. * $P < 0.05$ compared with the corresponding group.

quitously expressed, the toxicity of TBT might be observed in various cell types. Several TCA cycle enzymes have been reported to contribute to cell proliferation. For example, NADP-IDH plays a role for cell growth under hypoxic conditions in human glioblastoma cells[26]. Another study has shown that aconitase mediated cell proliferation via ATP production in human prostate carcinoma cells[27]. NAD-IDH has been shown to regulate the metabolic fluxes and the generation of ATP in the TCA cycle[28]. Therefore, it is likely that NAD-IDH is a target of TBT cytotoxicity and regulates cell growth in embryonic carcinoma cells.

In addition to cell growth inhibition, we also showed that neural differentiation is enhanced by TBT exposure or NAD-IDH inhibition (Figure 3). Consistent with our data, overexpression of NAD-IDHα has been shown to reduce neuronal differentiation and neurite outgrowth through the inactivation of MAPK phosphorylation in PC12 cells[29]. Because TBT exposure has been reported to induce neurotoxicity via ERK and p38MAPK phosphorylation in cultured rat cortical neurons[30], TBT exposure might cause cytotoxicity through the MAPK pathways. Thus, a non-genomic pathway plays a role in TBT toxicity. Indeed, the genomic target PPARγ and treatment with cycloheximide did not alter the effects of TBT (Figure S1–3). It is unlikely that transcriptional regulation is involved in NAD-IDH activity and the enhancement of neuronal differentiation. The downstream pathway of TBT-NAD-IDH should be determined in embryonic carcinoma cells.

Our data suggest that TBT regulates NAD-IDH activity through possible interaction. However, we can not conclude that it is through direct binding. Previous reports have suggested that TBT can bind to multiple target proteins, such as PPARγ, RXR, F1F0 ATP synthase and 11β-hydroxysteroid dehydrogenase (11β-HSD) type 2, with broad specificity[19,31]. For example, TBT binds the RXRα ligand-binding domain through a covalent bond between the tin atom and the Cys residue[32]. TBT also binds 11β-HSD type 2 by interacting with several Cys residues in the active site[31]. Because the ligand-binding pocket of hNAD-IDHα contains several Cys residues[33] and has enough space to accommodate TBT, TBT might bind to hNAD-IDHα via Cys residues. Future conformational analysis, including X-ray crystallography or computer simulation, and mutagenesis studies should be performed to determine whether TBT binds to hNAD-IDHα or not.

Our metabolomic analysis showed that TBT inhibited cell growth and enhanced neuronal differentiation through possible direct

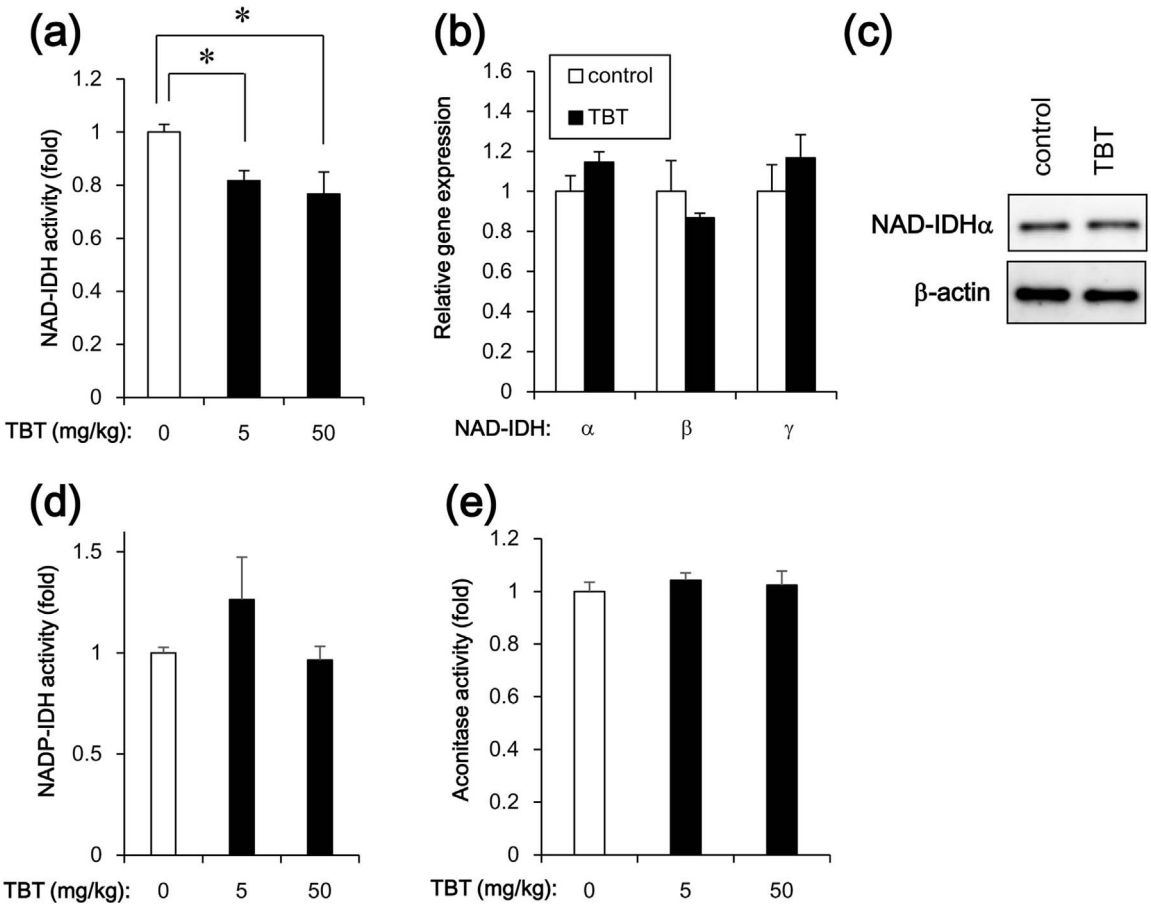

Figure 4 | NAD-IDH enzyme activity in the brain of rats orally exposed to TBT at doses of 5 and 50 mg/kg for 6 h. (a) NAD-IDH activity was determined in the brain lysates. (b) The relative expression levels of NAD-IDHα, β, and γ in rats exposed to 50 mg/kg TBT were measured using real-time PCR. The relative changes were normalized to the levels of RPL13. (c) The expression of NAD-IDHα protein was examined by western blot analysis using the anti-NAD-IDHα and anti-β-actin antibodies. Cropped blots were shown and the full-length blots were indicated in Supplementary Fig. 4. (d) NADP-IDH activity was determined in the brain lysates. (e) Aconitase activity was determined in the brain lysates. * $P < 0.05$ compared with the corresponding TBT 0 group.

inhibition of NAD-IDH activity in human embryonic carcinoma cells. Thus, comprehensive approach of non-genomic metabolic pathway might be a powerful tool to elucidate the mechanism of EDC action.

Methods

Chemicals and reagents. TBT was obtained from Tokyo Chemical Industry (Tokyo, Japan). Tin acetate (TA) and rosiglitazone were obtained from Sigma-Aldrich (St. Louis, MO, USA). All other reagents were of analytical grade and were obtained from commercial sources.

Cell culture. NT2/D1 cells were obtained from the American Type Culture Collection. The cells were cultured in Dulbecco's modified Eagle's medium (DMEM; Sigma-Aldrich) supplemented with 10% fetal bovine serum (FBS; Biological Industries, Ashrat, Israel) and 0.05 mg/ml penicillin-streptomycin mixture (Life Technologies, Carlsbad, CA, USA) at 37°C and 5% CO2. For neural differentiation, all-trans retinoic acid (RA; Sigma-Aldrich) was added to the medium twice a week at a final concentration of 10 μM.

Determination of TCA cycle metabolites. Intracellular metabolites were extracted and used for subsequent capillary electrophoresis time-of-flight mass spectrometry (CE-TOFMS) analysis, as previously described. The amounts of the metabolites were determined using an Agilent CE capillary electrophoresis system (Agilent Technologies, Waldbronn, Germany) equipped with an Agilent G3250AA LC/MSD TOF system (Agilent Technologies, Palo Alto, CA), an Agilent 1100 series isocratic HPLC pump, a G1603A Agilent CE-MS adapter kit, and a G1607A Agilent CE-electrospray ionization 53-MS sprayer kit. For system control and data acquisition, the G2201AA Agilent ChemStation software was used for CE, and the Agilent TOF (Analyst QS) software was used for the TOFMS.

Measurement of intracellular ATP levels. The intracellular ATP content was measured using the ATP Determination Kit (Life Technologies), according to the manufacturer's protocol. Briefly, the cells were washed and lysed with 0.1% Triton X-100/PBS. The resulting cell lysates were added to a reaction mixture containing 0.5 mM D-luciferin, 1 mM DTT, and 1.25 μg/ml luciferase and incubated for 30 min at room temperature. Luminescence was measured using a Wallac1420ARVO fluoroscan (Perkin-Elmer, Waltham, MA, USA). The luminescence intensities were normalized to the total protein content.

Isocitrate dehydrogenase (IDH) activity assay. IDH activity was determined using the commercial Isocitrate Dehydrogenase Activity Colorimetric Assay Kit (Biovision, Mountain View, CA, USA), according to the manufacturer's instructions. Briefly, NT2/D1 cells were lysed in an assay buffer provided in the kit. The lysate was centrifuged at 14,000 g for 15 min, and the cleared supernatant was used for the assay. NADP or NAD was used as the substrate for the NADP-IDH or NAD-IDH assay, respectively.

Real-time PCR. Total RNA was isolated from NT2/D1 cells using the TRIzol reagent (Life Technologies), and quantitative real-time reverse transcription (RT)-PCR with the QuantiTect SYBR Green RT-PCR Kit (QIAGEN, Valencia, CA, USA) was performed using an ABI PRISM 7900HT sequence detection system (Applied Biosystems, Foster City, CA, USA), as previously reported. The relative changes in the transcript amounts of each sample were normalized to the mRNA levels of ribosomal protein L13 (RPL13). The following primer sequences were used for real-time PCR analysis: human NAD-IDHα: forward, 5′-ATCGGAGGTCTCGGTGTG-3′, reverse, 5′-AGGAGGGCTGTGGGATTC-3′; human NAD-IDHβ: forward, 5′-GCCTC-AGCCGCATATCATAG-3′, reverse, 5′-GAGCAGGTGCTGAGTTCCAT-3′; human NAD-IDHγ: forward, 5′-TTAGCGGACGGAGGAATTGT-3′, reverse, 5′-CAGCCCTTCTCTGCCGT-3′; human NeuroD: forward, 5′-GGAAACGA-ACCCACTGTGCT-3′, reverse, 5′-GCCACACCAAATTCGTGGTG-3′; human Math1: forward, 5′-GTCCGAGCTGCTACAAACG-3′, reverse, 5′-GTGGTGGT-GGTCGCTTTT-3′; human RPL13: forward, 5′-CATCGTGGCTAAACAGGTAC-

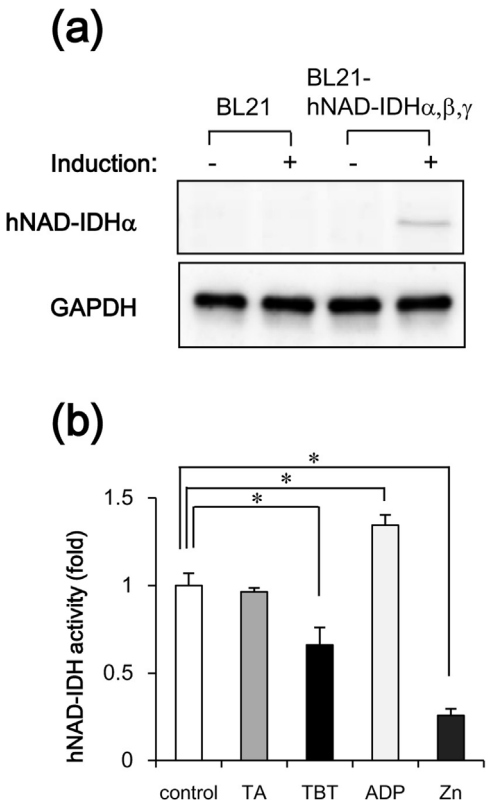

Figure 5 | Reduction of NAD-IDH enzyme activity by interaction with TBT in an E. coli expression system. (a) After the expression of pHIDHα, β, γ was induced by culturing E. coli BL21 transformants at 25°C for 20 h, crude extracts were prepared and were subjected to western blot analysis using the anti-NAD-IDHα and anti-GAPDH antibodies. Cropped blots were shown and the full-length blots were indicated in Supplementary Fig. 4. (b) After treatment with 100 nM TBT for 1 h, NAD-IDH activity was determined in the crude extracts. ADP (100 μM) and Zn^{2+} (2 mM) were used as positive and negative controls, respectively. * $P < 0.05$ compared with the corresponding control group.

TG-3′, reverse, 5′-GCACGACCTTGAGGGCAGCC-3′; rat NAD-IDHα: forward, 5′-TGGGTGTCCAAGGTCTCTC-3′, reverse, 5′-CTCCCACTGAATAGGTG-CTTTG-3′; rat NAD-IDHβ: forward, 5′-AGGCACAAGATGTGAGGGTG-3′, reverse, 5′-CAGCAGCCTTGAACACTTCC-3′; rat NAD-IDHγ: forward, 5′-TGGGCGGCATACAGTGACTA-3′, reverse, 5′-TTGGAGCTTACATGCAC-CTCT-3′; rat RPL13: forward, 5′-GGCTGAAGCCTACCAGAAAG-3′, reverse, 5′-CTTTGCCTTTTCCTTCCGTT-3′.

Aconitase activity assay. Aconitase activity was determined using the commercial Aconitase Activity Colorimetric Assay Kit (Biovision), according to the manufacturer's instructions. Briefly, NT2 cells were lysed in an assay buffer provided in the kit. The lysate was centrifuged at 14,000 g for 15 min, and the cleared supernatant was used for the aconitase assay.

NAD-IDHα knockdown experiment. Transient gene knockdown was performed using NAD-IDHα shRNA lentiviruses from Sigma-Aldrich (MISSION® shRNA) according to manufacturer's protocol. A scrambled hairpin sequence was used as a negative control. Briefly, the cells were infected with the viruses at a multiplicity of infection of 10, in the presence of 8 μg/ml hexadimethrine bromide (Sigma-Aldrich), for 24 h, and were then subjected to selection with 0.5 μg/ml puromycin for 72 h prior to functional analyses.

Tissue preparation. The present study was approved by the animal ethics committee and was conducted in accordance with the regulations on the use of living modified organisms of Hiroshima University. Male Slc:Wistar/ST rats (8 weeks old) were purchased from Japan SLC, Inc. (Shizuoka, Japan). They were housed under controlled temperature, 12 h light/dark cycle, and humidity (75 ± 5%) for at least 1 week prior to experiments. Standard pellet food and water were provided ad libitum. TBT solution (5 and 50 mg/kg body weight) was orally administered to rats. TBT was dissolved in polyethylene glycol. The whole brain was exposed by the use of fine scissors and forceps, and the frontal part of cerebral cortex was excised from the brain.

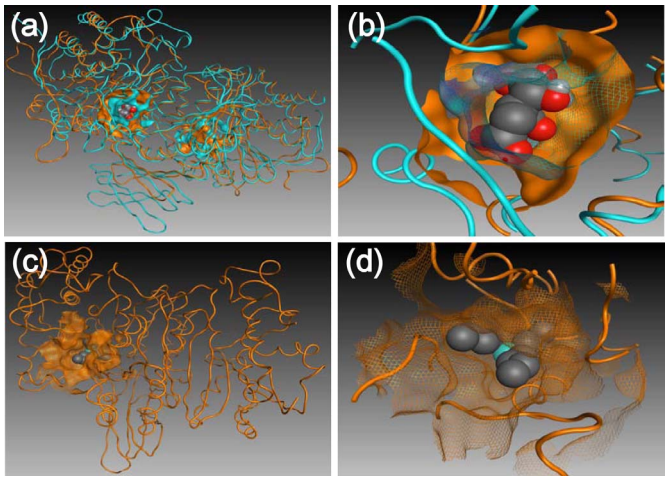

Figure 6 | *In silico* docking simulation analysis. (a) Overlaid structures of the calculated hNAD-IDHα (orange) and hNADP-IDH (cyan) homodimers bound to isocitric acid (Space-filling model). (b) The ligand binding pockets of the hNAD-IDHα (solid) and hNADP-IDH (wireframe) proteins. (c, d) Docking structure of hNAD-IDHα containing TBT (Space-filling model).

Transformation and Expression of Recombinant Human NAD-IDH Proteins in E. coli. pHIDHαβ1γ plasmid DNA (a kind gift from Dr. T. L. Huh) was used to transform E. coli BL21 (DE3) ultracompetent cells (BioDynamics, Tokyo, Japan). The colonies with positive inserts were subcultured and grown overnight at 37°C in LB medium (2 ml) supplemented with ampicillin (0.1 mg/ml). To express the enzyme, 15 ml tubes containing 2 ml of LB medium with 0.1 mg/ml ampicillin were inoculated with freshly grown E. coli cells (1% v/v), and these cultures were grown at 37°C while being shaken at 220 rpm for 4 h. The flasks were then temporarily placed in chilled water to lower the culture temperature to 25°C. Protein expression was induced in the cells by shaking at a lower speed of 140 rpm with minimal aeration at 25°C for 20 h. Then, 2 ml of the cell culture was centrifuged at 6,000 g for 15 min to separate the cells from the media, and the pellet was suspended in a total volume of 300 μl of cold assay buffer, a component of Isocitrate Dehydrogenase Activity Assay Kit. The suspended cells were subjected to 3 cycles of freeze-thaw before sonication (5 cycles of 15 sec sonication and 45 sec rest) and lysed. The cell lysate was centrifuged at 14,000 g for 15 min, and the cleared supernatant (crude extract) was separated. Recombinant human NAD-IDH activity was determined by subtracting basal activity in the crude extract from control BL21 cells.

Western blot analysis. Western blot analysis was performed as previously reported[34]. Briefly, the cells were lysed with Cell Lysis Buffer (Cell Signaling Technology, Danvers, MA, USA), and the proteins were separated by sodium dodecyl sulfate (SDS)-polyacrylamide gel electrophoresis and electrophoretically transferred to Immobilon-P (Millipore, Billerica, MA, USA). The membranes were probed with an anti-NAD-IDH (IDH3) α polyclonal antibody (1 : 1,000; Abcam, Cambridge, UK), an anti-β-actin monoclonal antibody (1 : 5,000; Sigma-Aldrich), and an anti-GAPDH monoclonal antibody (1 : 2,000; Abcam). The membranes were then incubated with secondary antibodies against rabbit or mouse IgG conjugated to horseradish peroxidase (Cell Signaling Technology). The bands were visualized using the ECL Western Blotting Analysis System (GE Healthcare, Buckinghamshire, UK), and the images were acquired using a LAS-3000 Imager (FUJIFILM UK Ltd., Systems, Bedford, UK). The density of each band was quantified using the ImageJ software (NIH, Bethesda, MD, USA).

In silico docking simulation studies. Homology modeling and docking studies of the human NAD-IDHα (hNAD-IDHα) and NADP-IDH (hNADP-IDH) homodimers were performed using Molecular Operating Environment (MOE) 2012.10. The models of hNAD-IDHα and hNADP-IDH were constructed based on the crystallographic structure of the porcine NADP-IDH homodimer (PDB: 1LWD)[35] using the standard protocols in MOE 2012.10. The docking simulations of the TBT-bound hNAD-IDHα and hNADP-IDH were carried out using ASEDock[36]. The TBT ligand was assigned in ASEDock, and the conformations were calculated using MMFF94S force field[37].

Statistical analysis. Results are shown as mean ± S.D. Statistical analysis was performed using one-way ANOVA followed by Dunnett's test. Differences at $P < 0.05$ were considered to be significant.

1. Toppari, J. *et al.* Male reproductive health and environmental xenooestrogens. *Environ. Health Perspect.* **104**, 741–803 (1996).

2. Hall, J. M. & Korach, K. S. Analysis of the molecular mechanisms of human estrogen receptors alpha and beta reveals differential specificity in target promoter regulation by xenoestrogens. *J. Biol. Chem.* **277**, 44455–44461 (2002).
3. Newbold, R. R., Padilla-Banks, E. & Jefferson, W. N. Adverse Effects of the Model Environmental Estrogen Diethylstilbestrol Are Transmitted to Subsequent Generations. *Endocrinology* **147**, s11–17 (2006).
4. Bulayeva, N. N., Gametchu, B. & Watson, C. S. Quantitative measurement of estrogen-induced ERK 1 and 2 activation via multiple membrane-initiated signaling pathways. *Steroids* **69**, 181–192 (2004).
5. Liu, D., Homan, L. L. & Dillon, J. S. Genistein acutely stimulates nitric oxide synthesis in vascular endothelial cells by a cyclic adenosine 5′-mono-phosphate-dependent mechanism. *Endocrinology* **145**, 5532–5539 (2004).
6. Watson, C. S., Alyea, R. A., Jeng, Y. J. & Kochukov, M. Y. Nongenomic actions of low concentration estrogens and xenoestrogens on multiple tissues. *Mol. Cell Endocrinol.* **274**, 1–7 (2007).
7. Bredfeldt, T. G. *et al.* Xenoestrogen-induced regulation of EZH2 and histone methylation via estrogen receptor signaling to PI3K/AKT. *Mol. Endocrinol.* **24**, 993–1006 (2010).
8. Gardlund, A. T. *et al.* Effects of prenatal exposure to tributyltin and trihexyltin on behavior in rats. *Neurotoxicol. Teratol.* **13**, 99–105 (1991).
9. Noda, T. *et al.* Teratogenicity study of tri-n-butyltin acetate in rats by oral administration. *Toxicol. Lett.* **55**, 109–115 (1991).
10. Whalen, M. M., Loganathan, B. G. & Kannan, K. Immunotoxicity of environmentally relevant concentrations of butyltins on human natural killer cells in vitro. *Environ Res.* **81**, 108–116 (1999).
11. Matthiessen, P. & Gibbs, P. E. Critical appraisal of the evidence for tributyltin mediated endocrine disruption in mollusks. *Environ. Toxicol. Chem.* **17**, 37–43 (1998).
12. McAllister, B. G. & Kime, D. E. Early life exposure to environmental levels of the aromatase inhibitor tributyltin causes masculinisation and irreversible sperm damage in zebrafish (Danio rerio). *Aquat. Toxicol.* **65**, 309–316 (2003).
13. Nishikawa, J. *et al.* Involvement of the retinoid X receptor in the development of imposex caused by organotins in gastropods. *Environ. Sci. Technol.* **38**, 6271–6276 (2004).
14. Kanayama, T., Kobayashi, N., Mamiya, S., Nakanishi, T. & Nishikawa, J. Organotin compounds promote adipocyte differentiation as agonists of the peroxisome proliferator-activated receptor gamma/retinoid X receptor pathway. *Mol. Pharmacol.* **67**, 766–774 (2005).
15. Grün, F. *et al.* Endocrine-disrupting organotin compounds are potent inducers of adipogenesis in vertebrates. *Mol. Endocrinol.* **20**, 2141–2155 (2006).
16. Cooke, G. M. Effect of organotins on human aromatase activity in vitro. *Toxicol. Lett.* **126**, 121–130 (2002).
17. Doering, D. D., Steckelbroeck, S., Doering, T. & Klingmüller, D. Effects of butyltins on human 5alpha-reductase type 1 and type 2 activity. *Steroids* **67**, 859–867 (2002).
18. McVey, M. J. & Cooke, G. M. Inhibition of rat testis microsomal 3beta-hydroxysteroid dehydrogenase activity by tributyltin. *J. Steroid Biochem. Mol. Biol.* **86**, 99–105 (2003).
19. von Ballmoos, C., Brunner, J. & Dimroth, P. The ion channel of F-ATP synthase is the target of toxic organotin compounds. *Proc. Natl. Acad. Sci. U S A* **101**, 11239–11244 (2004).
20. Yamada, S., Kotake, Y., Sekino, Y. & Kanda, Y. AMP-activated protein kinase-mediated glucose transport as a novel target of tributyltin in human embryonic carcinoma cells. *Metallomics* **5**, 484–491 (2013).
21. Vinekar, R., Verma, C. & Ghosh, I. Functional relevance of dynamic properties of Dimeric NADP-dependent Isocitrate Dehydrogenases. *BMC Bioinformatics* **13**, S2 (2012).
22. Birket, M. J. *et al.* A reduction in ATP demand and mitochondrial activity with neural differentiation of human embryonic stem cells. *J. Cell Sci.* **124**, 348–358 (2011).
23. Kim, Y. O. *et al.* Identification and functional characterization of a novel, tissue-specific NAD(+)-dependent isocitrate dehydrogenase β subunit isoform. *J. Biol. Chem.* **274**, 36866–36875 (1999).
24. Cohen, P. F. & Colman, R. F. Diphosphopyridine nucleotide dependent isocitratedehydrogenase from pig heart. Charactgerization of the active substrate and modes of regulation. *Biochemistry* **11**, 1501–1508 (1972).
25. Lemire, J., Mailloux, R. & Appanna, V. D. Zinc toxicity alters mitochondrial metabolism and leads to decreased ATP production in hepatocytes. *J. Appl. Toxicol.* **28**, 175–182 (2008).
26. Wise, D. R. *et al.* Hypoxia promotes isocitrate dehydrogenase-dependent carboxylation of α-ketoglutarate to citrate to support cell growth and viability. *Proc. Natl. Acad. Sci. U S A* **108**, 19611–19616 (2011).
27. Juang, H. H. Modulation of mitochondrial aconitase on the bioenergy of human prostate carcinoma cells. *Mol. Genet. Metab.* **81**, 244–252 (2004).
28. Gabriel, J. L., Zervos, P. R. & Plaut, G. W. Activity of purified NAD-specific isocitrate dehydrogenase at modulator and substrate concentrations approximating conditions in mitochondria. *Metabolism* **35**, 661–667 (1986).
29. Cho, S. A. *et al.* Up-regulation of Idh3alpha causes reduction of neuronal differentiation in PC12 cells. *BMB Rep.* **43**, 369–374 (2010).
30. Nakatsu, Y. *et al.* Glutamate excitotoxicity is involved in cell death caused by tributyltin in cultured rat cortical neurons. *Toxicol. Sci.* **89**, 235–242 (2006).
31. Atanasov, A. G., Nashev, L. G., Tam, S., Baker, M. E. & Odermatt, A. Organotins disrupt the 11beta-hydroxysteroid dehydrogenase type 2-dependent local inactivation of glucocorticoids. *Environ. Health Perspect.* **113**, 1600–1606 (2005).
32. le Maire, A. *et al.* Activation of RXR-PPAR heterodimers by organotin environmental endocrine disruptors. *EMBO Rep.* **10**, 367–373 (2009).
33. Kim, Y. O. *et al.* Characterization of a cDNA clone for human NAD(+)-specific isocitrate dehydrogenase alpha-subunit and structural comparison with its isoenzymes from different species. *Biochem. J.* **308**, 63–68 (1995).
34. Kanda, Y. & Watanabe, Y. Adrenaline increases glucose transport via a Rap1-p38MAPK pathway in rat vascular smooth muscle cells. *Br. J. Pharmacol.* **151**, 476–482 (2007).
35. Ceccarelli, C., Grodsky, N. B., Ariyaratne, N., Colman, R. F. & Bahnson, B. J. Crystal structure of porcine mitochondrial $NADP^+$-dependent isocitrate dehydrogenase complexed with Mn^{2+} and isocitrate. Insights into the enzyme mechanism. *J. Biol. Chem.* **277**, 43454–43462 (2002).
36. Goto, J., Kataoka, R., Muta, H. & Hirayama, N. ASEDock-docking based on alpha spheres and excluded volumes. *J. Chem. Inf. Model.* **48**, 583–590 (2008).
37. Halgren, T. A. MMFF VI. MMFF94s option for energy minimization studies. *J. Comput. Chem.* **20**, 720–729 (1999).

Acknowledgments

We thank Ms. Mami Kohno, Mr. Kyoichi Masuda, and Ms. Saki Tanaka (Graduate School of Biomedical and Health Sciences, Hiroshima University) for technical assistance in the animal experiment. This work was supported by a Grant-in-Aid for Scientific Research from the Ministry of Education, Culture, Sports, Science, and Technology, Japan (#23590322 to Y.K.), a Health and Labour Sciences Research Grant from the Ministry of Health, Labour and Welfare, Japan (Y.K.), and a grant from the Smoking Research Foundation (Y.K.).

Author contributions

S.Y. performed most of the experiments. Y.Ka. planned the project. S.Y., Y.S. and Y.Ka. wrote the manuscript. Y.Ko. performed the animal experiments. Y.D. and M.K. performed *In silico* docking simulation analysis. All authors reviewed the manuscript.

Additional information

Supplementary information accompanies this paper at http://www.nature.com/scientificreports

Competing financial interests: The authors declare no competing financial interests.

How to cite this article: Yamada, S. *et al.* NAD-dependent isocitrate dehydrogenase as a novel target of tributyltin in human embryonic carcinoma cells. *Sci. Rep.* **4**, 5952; DOI:10.1038/srep05952 (2014).